A NEW SENSITIVITY ANALYSIS AND SOLUTION METHOD FOR SCINTILLOMETER MEASUREMENTS OF AREA-AVERAGE TURBULENT FLUXES

By

Matthew Gruber

RECOMMENDED:

Xiangdong Zhang

Richard L. Collins

Gilberto J. Fochesatto
Advisory Committee Chair

Uma S. Bhatt
Chair, Department of Atmospheric Sciences

APPROVED:

Paul W. Layer
Dean, College of Natural Science and Mathematics

John C. Eichelberger
Dean of the Graduate School

Date

A NEW SENSITIVITY ANALYSIS AND SOLUTION METHOD FOR SCINTILLOMETER MEASUREMENTS OF AREA-AVERAGE TURBULENT FLUXES

A

THESIS

Presented to the Faculty

of the University of Alaska Fairbanks

in Partial Fulfillment of the Requirements

for the Degree of

MASTER OF SCIENCE

By

Matthew Gruber, B.S.

Fairbanks, Alaska

May 2013

Abstract

Scintillometer measurements of the turbulence inner-scale length l_o and refractive index structure function C_n^2 allow for the retrieval of large-scale area-averaged turbulent fluxes in the atmospheric surface layer. This retrieval involves the solution of the non-linear set of equations defined by the Monin-Obukhov similarity hypothesis. A new method that uses an analytic solution to the set of equations is presented, which leads to a stable and efficient numerical method of computation that has the potential of eliminating computational error. Mathematical expressions are derived that map out the sensitivity of the turbulent flux measurements to uncertainties in source measurements such as l_o. These sensitivity functions differ from results in the previous literature; the reasons for the differences are explored.

Table of Contents

List of Figures

Page

List of Appendices

Acknowledgements

In addition to acknowledgements following the manuscript, I here make personal acknowledgements. First of all I need to thank Erica whose love, support, and humor kept me grounded. I thank my family for supporting and encouraging me during difficult times as well as during good times. I thank Barbara Day for organizing and encouraging my progress even during rushed times. I owe gratitude to Dr. Richard Collins both directly and indirectly. His daily rushed hustle and bustle around the department had fortuitous side-effects: it was a routine mid-summer morning when a door came crashing and I over-heard "Where's my notebook # 6!?" that I went to the UAF book store, purchased several notebooks, labelled them, pushed aside my stacks of unbinded notes, and that day on the first three pages of "notebook #1" I solved a problem related to the manuscsript which had been gnawing at me for over a month. I thank the rest of the faculty in the Deparment of Atmospheric Science, the administration at the graduate school department, and especially my fellow students for their support; I look forward to having the opportunity to work with them on group projects in the future. I thank everyone who has been involved with the development of LaTeX and Linux, as well as the UAF researchers who have maintained a thesis template. I also thank Dean Paul Layer as well as Director Robert McCoy. I thank Dr. Javier Fochesatto for his advisorship, especially for letting me be a part of really enjoyable field campaigns. I thank Dr. Xiangdong Zhang for serving on my committee.

The manuscript represents work produced by myself and Dr. Javier Fochesatto, with editing help from Dr. Peter Bieniek and (soon to be Dr.) Derek Starkenburg.

1 Introduction

1.1 Atmospheric Boundary Layer Turbulent Fluxes

Energy and momentum exchange between the Earth's crust and its atmosphere occurs at the Earth's surface. Before energy and momentum can be re-distributed by large scale atmospheric flows, they pass through a layer of air which interacts directly with the ground. Due to surface roughness and convection, the atmospheric flow forms a boundary layer near the ground. This atmospheric boundary layer typically has a depth of between a few meters to a couple of kilometers, and the bottom portion is deemed the surface layer. In the surface layer, turbulence due to thermal and humidity gradients and mechanical shearing dominates the process of energy, water, and momentum exchange.

Vertical turbulent surface layer fluxes of sensible heat, latent heat and momentum are important to measure for the validation of ecological, atmospheric, and large scale climate models [e.g., *Beyrich et al.*, 2002; *Marx et al.*, 2008]. These turbulent fluxes represent temporally averaged bulk movement of extensive quantities through imaginary horizontal planar surfaces above the terrain [e.g., *Sorbjan*, 1989]. As pressure is a single quantity which is a measure of the momentum transfer of countless molecular collisions and electromagnetic interactions [e.g. *Schroeder*, 2000], turbulent fluxes are singular quantities which represent statistical averages of some aspect of the movements of countless molecules and their associated energies and inertia.

On the scales that will be discussed here, the continuum approximation is valid; this is the realm of classical physics. While in theory the heat fluxes could be calculated by solving for the fluid flow and thermodynamics of the entire three dimensional field of the atmospheric surface layer in time, this is highly impractical. First of all, the equations which

describe such processes are the thermodynamic equations coupled to the Navier-Stokes equations, neglecting non-inertial reference frame effects such as the Coriolis effect. The Navier-Stokes equations follow from the fundamental Newton's laws applied to a continuous fluid, with the introduction of viscosity to take into account the electromagnetic interactions of passing (shearing) particles [e.g., *Landau and Lifshitz*, 1959]. While it is possible with known boundary conditions to numerically solve the Navier-Stokes equations, there is no known general solution to them. Furthermore, in practice the entire set of boundary conditions cannot be realistically measured with a high degree of accuracy. As such, equations are desired which relate measureable quantities to the turbulent fluxes. These equations may be based on fundamental equations such as the Navier-Stokes equations, but they will describe the situation at a "higher" level, with less explicit information involved.

The Buckinham-Pi Theorem allows such "higher" level equations to be derived to represent physical processes such as turbulence as seen in *Sorbjan* [1989]. The functional form of the relationships between measureable variables can be inferred with assumptions about the physical process under study. This is accomplished through an analysis of the dimensionality of physical variables involved in the problem, and as such it can only work well if the right assumptions are made about the appropriate variables dominating the physical process. The functional relationships which can be derived through this theory generally involve unknown dimensionless functions which are resolved empirically, or which may be derived theoretically outside the context of Buckingham-Pi Theorem.

As an example of an application of the Buckinham-Pi Theorem, in the 1940's, Taylor used it to estimate the energy released from a nuclear bomb while the only data at his disposal was a series of photographs of the explosion with a spacial and temporal scale embedded [e.g., *Taylor*, 1950a,b]. With assumptions about the relations between key variables in explosions resulting from energy (not gas) suddenly released in a small area, he estimated the bomb payload energy to a high degree of accuracy. He accomplished this estimate without introducing any details about the payload of the bomb.

In the case of atmospheric boundary layer studies, the quantity which needs to be estimated is, for example, the area-average large scale sensible heat flux through the surface layer. As an analogy, the sensible heat flux is the payload energy, the exact details of the turbulence is the information which is hidden (the nuclear physics behind the bomb in the case of Taylor), and the theoretical relationships which relate the data to the sensible heat flux emerge from the Monin-Obukhov similarity hypothesis [e.g., *Sorbjan*, 1989]. The Monin-Obukhov similarity hypothesis is also derived from Buckinham-Pi theory; it originated in the 1950's and it has been applied frequently in boundary layer physics [e.g., *Wilson*, 2008]. The Monin-Obukhov similarity hypothesis is a model of energy and momentum exchange via turbulence in the surface layer of the atmosphere. It assumes that large scale effects such as the Coriolis effect and large scale advection are negligible, and it reduces turbulent motions in the surface layer to statistical variables which are related to each other via their physical dimensions, as well as through empirically resolved dimensionless functions. Turbulent kinetic energy is generated at the surface layer in the form of large eddies through conduction of heat from the ground and mechanical shearing of airflow. These large eddies subsequently break apart into smaller eddies in a cascading process until a critical eddy size at which point viscosity dissipates the kinetic energy into heat. This critical eddy size is called the turbulence inner scale length, denoted by l_o.

These dynamic interactions between the air and the surface are represented by scalar variables such as the friction velocity $u_\star$, the temperature and humidity scales $T_\star$ and $Q_\star$, and the Obukhov length L. These are statistical variables; they are only expected to satisfy Monin-Obukov theory if measured over a certain averaging time in homogeneous and stationary turbulence. These variables are defined as

$$u_\star = ((\overline{u'w'})^2 + (\overline{v'w'})^2)^{1/4} \tag{1.1}$$

$$T_\star = -\frac{\overline{w'T'}}{u_\star} \tag{1.2}$$

$$L = \frac{u_\star^2 T}{g\kappa T_\star} \tag{1.3}$$

where u, v and w are the east-west, north-south, and vertical wind components, g is gravitational acceleration, κ is the von Kármán constant, T is temperature (or virtual temperature if water vapor is present), and primes denote deviations from temporal average due to turbulence, while bars denote time averages as seen in *Sorbjan* [1989]. Dimensional analysis leads to the conclusion that many aspects of the surface layer are functions of $u_\star$ and $T_\star$, and of the dimensionless variable z/L (which is an indicator of dynamic stability). From dimensional analysis alone, the behaviour of the unknown functions of z/L can only be specified in asymptotic regimes [e.g., *Sorbjan*, 1989].

The turbulent fluxes of interest are given by

$$H_S = -\rho c_p u_\star T_\star \tag{1.4}$$

$$H_L = -L_v u_\star Q_\star \tag{1.5}$$

$$\tau = \rho u_\star^2 \tag{1.6}$$

where H_S is the sensible heat flux, H_L is the latent heat flux, τ is the momentum flux, c_p is the specific heat capacity at constant pressure, ρ is the density, and L_v is the heat of vaporization. Since ρ, c_p and L_v are direct functions of source measurement variables such as temperature T, pressure P, and humidity Q, the main difficulty in resolving, say, H_S, is to resolve $u_\star$ and $T_\star$. While it is possible to measure the turbulent components of wind and temperature directly in order to resolve $u_\star$ and $T_\star$ through Eqs. (1.1) and (1.2), this is not easily done over a large scale. Typical instruments for direct measurements of

turbulent components of wind and temperature are eddy covariance systems consisting of sonic anemometers, or fast gas measuring devices. These instruments are well established and reliable, however they have a relatively small footprint compared to the size of an agricultural field or a space-borne instrument's pixel resolution. There are two disadvantages with a small footprint: firstly the turbulence must be sampled for a long enough averaging time to sample the full spectrum of eddies, and secondly, the field site may be heterogeneous with gradients in fluxes. In order to measure turbulent fluxes at a larger scale, the turbulence itself can be sampled at a larger scale. As Taylor took "snapshots" of the atomic bomb explosion from a distance, variables which describe the turbulence statistically can be sampled at large scales. The variables which are recorded are the turbulent structure functions such as the structure function for temperature C_T^2, as well as the turbulence inner scale length l_o. Structure functions are described in *Tatarskii* [1961]; they are a statistical description of the strength and spacial frequency of inhomogeneities in the air due to turbulent perturbations.

Structure functions such as C_T^2, and the turbulence inner scale length l_o, along with other measurable quantities such as P and T, are related to the turbulent fluxes through the Monin-Obukhov similarity hypothesis by

$$\frac{C_T^2 z^{2/3}}{T_\star^2} = g(z/L) \tag{1.7}$$

$$\frac{\kappa z \varepsilon}{u_\star^3} = \phi(z/L) \tag{1.8}$$

where z is the height above the surface, ε is the rate at which energy is transferred from large eddies to smaller eddies (which is related to l_o for a given turbulence spectrum), and $g(z/L)$ and $\phi(z/L)$ are empirical dimensionless functions [e.g., *Sorbjan*, 1989; *Andreas*, 1992]. While the statistical variables $T_\star$ and $u_\star$ are assumed to be independent of height in the constant flux surface layer, C_T^2 and ε are functions of the height above the surface z. Generally the set of equations which resolve $T_\star$ and $u_\star$ are coupled. C_T^2 and l_o may be sampled over large areas through an instrumentation strategy called optical scintillation.

1.2 Scintillation

On a hot day, if one looks out over a vast field, distant objects viewed through the atmospheric surface layer often appear blurry and wavy; they dance in the air. This is an effect of turbulence. Mixing, diffusion, and swirling of eddies in the air create inhomogeneities in the temperature and humidity of the air. The index of refraction of the air is a function of temperature and humidity, thus it demonstrates rapidly evolving inhomogeneities over a vast range of spacial and temporal scales. A scintillometer records quantitative information about these inhomogeneities in the index of refraction by transmitting and receiving pulses of narrow-band photons through a significant path of surface layer turbulence. The photons are scattered by these inhomogeneities. With an assumption about the form of the turbulent spectrum, records of the statistics of the intensity of electromagnetic radiation received at the scintillometer can be converted into information about the structure function of the index of refraction of the air C_n^2, as well as the turbulence inner scale length l_o [e.g., *Tatarskii*, 1961; *Ochs and Wang*, 1974; *Hill*, 1988; *Sasiela*, 1994]. The electromagnetic wave equations which follow from the Maxwell equations are solved in a medium with a stochastically varying index of refraction for the cylindrical boundary conditions involved. The solution for a large aperture scintillometer is given by

$$\sigma_{ln(I)} = 4\pi^2 k^2 \int_0^{L_p} \int_0^{\infty} K \psi_n(K, C_n^2, l_o) \sin^2 \left(\frac{K^2 x (L_p - x)}{2kL_p} \right) dK dx \tag{1.9}$$

where $\sigma_{ln(I)}$ is the variance of the logarithm of the intensity at the receiving end of a coherent plane wave, k is the optical wavenumber, K is the turbulence spacial wavenumber, ψ_n is the turbulence spectrum, L_p is the propagation distance, and x is the position between the transmitter and receiver along the line of beam propagation [e.g., *Ochs and Wang*, 1974; *Hill*, 1988].

The area-average measurements of C_n^2 and l_o are a potential alternative to the direct measurement of turbulent components of wind, temperature and humidity. The large

footprint of scintillometers is ideal for studies on an ecosystem or basin scale such as in the LITFASS experiment [e.g., *Beyrich et al.*, 2002; *Beyrich and Mengelkamp*, 2006; *Meijninger et al.*, 2006]. Remote sensing of turbulence also avoids complications such as the instrument affecting airflow. However, these gains are not without complications. One such complication is the fact that some photon wavelengths have non-negligible absorption which may be a function of fluctuating variables such as humidity; this results in an over-estimation of C_n^2 [e.g., *Solignac et al.*, 2012]. This is solved, in some cases, with the application of dual transmitters, or with a selection of wavelengths which are essentially not absorbed. Another complication is the potential for "saturation" of the C_n^2 signal at a certain level of intensity fluctuations, above which C_n^2 is under-estimated [e.g., *Wang et al.*, 1978]. In some cases this can be resolved by raising the scintillometer to a higher height where the turbulence is more dissipated, or by shortening the beam propagation distance of the beam path. Both z and L are variables which are taken into account in the theoretical relations which translate the set of source measurements into turbulent fluxes.

The structure function of the index of refraction can be decomposed into its individual structure function components representing fluctuations in temperature and humidity as

$$C_n^2 = \frac{A^2(T,P,Q,\lambda)}{T^2} C_T^2 + \frac{2A(T,P,Q,\lambda)B(T,P,Q,\lambda)}{TQ} C_{TQ} + \frac{B(T,P,Q,\lambda)}{Q^2} C_Q^2 \tag{1.10}$$

where T is the average temperature in the air mass, Q is the average absolute humidity, P is the average pressure, λ is the wavelength of photons, and A and B are functions specific to the medium [e.g., *Andreas*, 1989]. As such, C_n^2 is a measure of how "blurry" objects appear when viewed at a specific wavelength through an air mass. It is thus not only a measure of the turbulence strength, but it is also a measure of how sensitive the index of refraction of the air is to perturbations in temperature and humidity. Since a scintillometer using a single wavelength only measures one value of C_n^2, three separate values of $C_{n_1}^2$, $C_{n_2}^2$ and $C_{n_3}^2$ can be measured at different wavelengths λ_1, λ_2 and λ_3 in order to resolve the values of the structure functions C_T^2, C_{TQ} and C_Q^2 in Eq. (1.10), if one of them cannot

otherwise be neglected or parametrized.

In order to resolve variables such as $T_\star$, the measured C_T^2 may be input into, for example, Eq. (1.7) along with the height z at which the C_T^2 was sampled at. This height z is important to resolve accurately, since it can be seen from Eq. (1.7) that C_T^2 dissipates nonlinearly in height. The simplest theoretical field site is that of a "nearly" flat area with homogeneous terrain properties such as roughness length, thermal properties, and water availability. In this case, a single value of z may be representative; the variability of z can be incorporated into its measurement uncertainty as considered in *Andreas* [1989] and *Andreas* [1992].

There are many types of scintillometers, some which measure only C_n^2 such as large and extra large aperture scintillometers [e.g., *Kohsiek et al.*, 2002; *Kleissl et al.*, 2008], and others such as displaced beam scintillometers which measure both C_n^2 and l_o [e.g., *Hill*, 1988; *Andreas*, 1992]. There are also many wavelengths used, from near infra-red to the radio end of the spectrum [e.g., *Andreas*, 1989, 1990; *de Bruin et al.*, 2002]. As such, there are many instrument strategies which have been deployed. In order to resolve the three components of Eq. (1.10) and a path averaged $u_\star$ measurement, a triple wavelength strategy may be considered in which one of the scintillometers is measuring l_o as well as C_n^2, and the other two scintillometers are measuring C_n^2 at other wavelengths. If two separate wavelengths are being used, the assumption that $C_{TQ} = \sqrt{C_T^2 C_Q^2}$ is made in order to resolve Eq. (1.10) for each value of C_n^2 [e.g., *Andreas*, 1989]. When using a single wavelength, the index of refraction at this wavelength should only be influenced by temperature fluctuations in order to measure the sensible heat flux. In this case the latent heat flux can be inferred by measuring radiative and ground storage energy flux terms, and by invoking energy conservation while assuming that there is negligible advection of energy and storage of energy in chemical potential in the vegetation [*Monteith and Unsworth*, 2008].

If none of the scintillometers being used measures l_o, then the friction velocity $u_\star$ can either be measured at a small footprint scale by an eddy covariance system near the center

of the beam path, or it can be a partially path-averaged measurement by invoking the Businger-Dyer relation given by

$$u_\star = \frac{\kappa u(z_1)}{ln(z_1/z_0) - \psi_m(z_1/l) + \psi_m(z_0/l)} \tag{1.11}$$

where $u(z_1)$ is the wind speed at height z_1, z_0 is the roughness length (or effective roughness length over variable terrain), and ψ_m is a unit-less similarity function [e.g., *Panofsky and Dutton*, 1984; *Sorbjan*, 1989; *Solignac et al.*, 2009]. While $u(z_1)$ is a point measurement, L is still resolved in this case mostly at the path length scale through the rest of the coupled equations in the set by incorporating C_n^2. This feature of mixing point source measurements such as T and P with path averaged source measurements such as C_n^2 and l_o is unavoidable in scintillometer strategies. The assumption of representativity of point measurements such as T on the whole beam path scale may introduce systematic error which is temporally evolving. This problem can be treated alongside general uncertainty analyses.

In previous studies, the coupled set of equations relating $u_\star$, $T_\star$, and $Q_\star$ to L via knowledge of the structure functions and l_o has been solved via an iterative algorithm in which many variables are free to change, and in which convergence is assumed upon reaching a cut-off value for relative change between successive iterations. [e.g., *Andreas*, 1989; *Lagouarde et al.*, 2002; *Hartogensis et al.*, 2003; *Solignac et al.*, 2009].

1.3 Uncertainty Propagation

Knowledge of the uncertainty of measurements is important for comparison of data with hypotheses based on theory. Much focus is placed on uncertainty in numerical weather prediction and climate forecasting. Uncertainty propagates from measurements through atmospheric models to the model output in sometimes surprising ways due to the inherrent nonlinearity the large set of equations involved.

Scintillometer measurement techniques involve a set of coupled equations with vari-

ables that are representative of varying scales. Uncertainty analyses are thus both crucial, and difficult. The distinction can be made between two types of variables: source measurements, and derived variables. Source measurements are either those variables which are measured directly, or they are calculated from variables which are independent of the rest of the source measurements (i.e., C_n^2 is calculated from $\sigma_{ln(I)}$, however C_n^2 can be considered to be a source measurement). Derived variables are those which are calculated from the source measurements via the set of (coupled) equations.

There are two types of errors possible on source measurements: systematic, and random. Random error is easiest to deal with when it is independent and Gaussian distributed. In this case, error is propagated from the source measurements to the derived variables by

$$\sigma_f = \sum_{i=1}^{N} \left(\frac{\partial f}{\partial x_i} \right) \sigma_{x_{s_i}} + \sqrt{\sum_{i=1}^{N} \left(\frac{\partial f}{\partial x_i} \right)^2 \sigma^2_{x_{r_i}}} + \sigma_{f_c}, \tag{1.12}$$

where the derived variable f is a function of source measurement variables $x_1, x_2, ..., x_N$ with respective systematic error $\sigma_{x_{s_1}}, \sigma_{x_{s_2}}, ..., \sigma_{x_{s_N}}$ and with respective independent Gaussian distributed uncertainties with standard deviations $\sigma_{x_{r_1}}, \sigma_{x_{r_2}}, ..., \sigma_{x_{r_N}}$ as seen in *Taylor* [1997]. The numerical indices indicate different independent variables, such as T, p, or z, for example. Computational error f due to the inaccurate solution of the theoretical equations is represented by σ_{f_c}. The first and last terms in Eq. 2.29 represent an offset from the true solution (inaccuracy), whereas the central square-root term represents the breadth of uncertainty due to random error (imprecision). Even in more complicated cases involving correlated errors, partial derivatives in equations similar to Eq. (1.12) must still be solved for as seen in *Taylor* [1997]. From a mathematical perspective, source measurements are independent variables, and derived variables are dependent variables.

The solution of Eq. (1.12) can be pursued numerically or analytically. Monte Carlo numerical analyses have been produced for the equations involved with scintillometer measurements of turbulent fluxes as seen in *Moroni et al.* [1990]. If the problem is approached

analytically, total differential expansions may be used to solve for the partial derivative terms in Eq. (1.12 as seen in, for example, *Andreas* [1989] and *Andreas* [1992]. Otherwise, the partial derivatives may be evaluated directly as seen in, for example, *Hartogensis et al.* [2003].

1.4 Thesis Goals and Outline

One goal of this thesis is to introduce efficient and accurate methods of solution of the turbulent heat fluxes which eliminate computational error. Another goal is to introduce new methods of solution for sensitivity functions in order to investigate error propagation in scintillometer strategies, as well as to reduce these functions to a closed, compact form for routing data analysis. Another goal is to take the first step to expanding previous studies of uncertainty propagation to the more realistic case of variable topography.

The manuscript (chapter 2) focuses on new and improved methods of solution and uncertainty analysis for scintillometer deployment over flat and homogeneous terrain. A focus is made on displaced-beam scintillometers which measure path averaged friction velocity $u_\star$. General conclusions are made in chapter 3.

Bibliography

Andreas, E. (1989), Two-wavelength method of measuring path-averaged turbulent surface heat fluxes, *Journal Of Atmospheric and Oceanic Technology*, *6*, 280–292.

Andreas, E. (1990), Three-wavelength method of measuring path-averaged turbulent heat fluxes, *Journal Of Atmospheric and Oceanic Technology*, *7(6)*, 801–814.

Andreas, E. (1992), Uncertainty in a path averaged measurement of the friction velocity $u_\star$, *Journal Of Applied Meteorology*, *31*, 1312–1321.

Beyrich, F., and H.-T. Mengelkamp (2006), Evaporation over a heterogeneous land surface: EVA-GRIPS and the LITFASS-2003 experiment - an overview, *Boundary Layer Meteorology*, *121*, 5–32.

Beyrich, F., H. de Bruin, W. Meijninger, J. Schipper, and H. Lohse (2002), Results from one-year continuous operation of a large aperture scintillometer over a heterogeneous land surface, *Boundary Layer Meteorology*, *105*, 85–97.

de Bruin, H., W. Meijninger, A.-S. Smedman, and M. Magnusson (2002), Displaced-beam small aperture scintillometer test. Part 1: The WINTEX data-set, *Boundary Layer Meteorology*, *105*, 129–148.

Hartogensis, O., C. Watts, J.-C. Rodriguez, and H. de Bruin (2003), Derivation of an effective height for scintillometers: La Poza experiment in Northwest Mexico, *Journal Of Hydrometeorology*, *4*, 915–928.

Hill, R. (1988), Comparison of scintillation methods for measuring the inner scale of turbulence, *Journal Of Applied Optics*, *27(11)*, 2187–2193.

Kleissl, J., J. Gomez, S.-H. Hong, J. Hendrickx, T. Rahn, and W. Defoor (2008), Large aperture scintillometer intercomparison study, *Boundary Layer Meteorology*, *128*, 133–150.

Kohsiek, W., W. Meijninger, A. Moene, B. Heusinkvel, O. Hartogensis, W. Hillen, and H. De Bruin (2002), An extra large aperture scintillometer for long range applications, *Boundary Layer Meteorology*, *105*, 119–127.

Lagouarde, J., J. Bonnefond, Y. Kerr, K. McAneney, and M. Irvine (2002), Integrated sensible heat flux measurements of a two-surface composite landscape using scintillometry, *Boundary Layer Meteorology*, *105*, 5–35.

Landau, L., and E. Lifshitz (1959), *Course of Theoretical Physics, Volume 6: Fluid Mechanics*, Pergamon Press, New York, United States, 536 pp.

Marx, A., H. Kunstmann, D. Schuttemeyer, and A. Moene (2008), Uncertainty analysis for satelite derived sensible heat fluxes and scintillometer measurements over savannah environment and comparison to mesoscale meteorological simulation results, *Agricultural Forest Meteorology*, *148*, 656–667.

Meijninger, W., F. Beyrich, L. A., W. Kohsiek, and H. de Bruin (2006), Scintillometer-based turbulent fluxes of sensible and latent heat over a heterogeneous land surface - a contribution to LITFASS-2003, *Boundary Layer Meteorology*, *121*, 89–110.

Monteith, J., and M. Unsworth (2008), *Environmental Physics, 3rd Edition*, Academic Press, Massachussets, United States, 440 pp.

Moroni, C., A. Navarra, and R. Guzzi (1990), Estimation of the turbulent fluxes in the surface layer using the inertial dissipative method: A Monte Carlo error analysis, *Boundary Layer Meteorology*, *50*, 339–354.

Ochs, G., and T.-I. Wang (1974), Finite aperture scintillometer for profiling wind and C_n^2, *Journal of Applied Optics*, *17*, 3774–3778.

Panofsky, H., and J. Dutton (1984), *Atmospheric Turbulence: Models and Methods for Engineering Applications*, J. Wiley, New York, United States, 397 pp.

Sasiela, R. (1994), *Electromagnetic Wave Propagation in Turbulence: Evaluation and Application of Mellin Transforms*, Springer-Verlag, 300 pp.

Schroeder, D. (2000), *An Introduction to Thermal Physics*, Addison Wesley Longman, California, United States, 422 pp.

Solignac, P., A. Brut, J.-L. Selves, J.-P. Béteille, J.-P. Gastellu-Etchegorry, P. Keravec, P. Béziat, and E. Ceschia (2009), Uncertainty analysis of computational methods for deriving sensible heat flux values from scintillometer measurements, *Journal Of Atmospheric Measurement Techniques*, *2*, 741–753.

Solignac, P., A. Brut, J.-L. Selves, J.-P. Béteille, and J.-P. Gastellu-Etchegorry (2012), Attenuating the absorption contribution on C_n^2 estimates with a large aperture scintillometer, *Boundary Layer Meteorology*, *143*, 261–283.

Sorbjan, Z. (1989), *Structure of the Atmospheric Boundary Layer*, Prentice Hall, New Jersey, United States, 317 pp.

Tatarskii, V. (1961), *Wave Propagation in a Turbulent Medium*, McGraw-Hill Book Company, New York, United States, 285 pp.

Taylor, G. (1950a), The formation of a blast wave by a very intense explosion. I. Theoretical discussion, *Proceedings of the Royal Society of London, Series A, Mathematical and Physical Sciences*, *201(1065)*, 159–174.

Taylor, G. (1950b), The formation of a blast wave by a very intense explosion. II. The atomic explosion of 1945, *Proceedings of the Royal Society of London, Series A, Mathematical and Physical Sciences*, *201(1065)*, 175–186.

Taylor, J. (1997), *An Introduction to Error Analysis: The Study of Uncertainties in Physical Measurements, 2nd Edition*, University Science Books, California, United States, 327 pp.

Wang, T., G. Ochs, and S. Clifford (1978), Saturation-resistant optical scintillometer to measure C_n^2, *Journal of Optical Society of America*, *68*, 334–338.

Wilson, J. (2008), Monin-Obukhov functions for standard deviations of velocity, *Boundary Layer Meteorology*, *129*, 353–369.

2 A New Sensitivity Analysis and Solution Method for Scintillometer Measurements of Area-Average Turbulent Fluxes [1]

Abstract

Scintillometer measurements of the turbulence inner-scale length l_o and refractive index structure function C_n^2 allow for the retrieval of large-scale area-averaged turbulent fluxes in the atmospheric surface layer. This retrieval involves the solution of the non-linear set of equations defined by the Monin-Obukhov similarity hypothesis. A new method that uses an analytic solution to the set of equations is presented, which leads to a stable and efficient numerical method of computation that has the potential of eliminating computational error. Mathematical expressions are derived that map out the sensitivity of the turbulent flux measurements to uncertainties in source measurements such as l_o. These sensitivity functions differ from results in the previous literature; the reasons for the differences are explored.

[1] In press *Boundary Layer Meteorology*, M. Gruber and G. J. Fochesatto.

2.1 Introduction

Scintillometers detect fluctuations in the intensity of a beam of light that passes through a path length of 50 m to 5000 m of near-ground turbulence in the surface layer [*Kleissl et al.*, 2008]. These fluctuations are related to the structure function of the index of refraction C_n^2, and the turbulence inner-scale length l_o [*Tatarskii*, 1961; *Hill*, 1988; *Sasiela*, 1994]. The index of refraction is a function of temperature and humidity; thus C_n^2 can be decomposed into structure functions of temperature T and humidity q as C_T^2, C_{Tq} and C_q^2. Scintillometer wavelengths are selected that are each more sensitive to fluctuations in one variable (such as temperature) than others (such as humidity), so that C_T^2, C_{Tq} and C_q^2 may be resolved. For example, intensity fluctuations of visible and near-infrared beams are more sensitive to temperature fluctuations than humidity fluctuations, while microwave beams are more sensitive to humidity fluctuations [*Andreas*, 1990]. Structure functions such as C_n^2 are described in *Tatarskii* [1961], and represent the strength and spacial frequency of perturbations in variables; thus C_n^2 is a measure of turbulence intensity weighted by the susceptibility of the index of refraction of the medium to changes in variables such as temperature and humidity.

The goal of this study is to solve for the sensible heat flux H_S and the momentum flux τ as functions of source measurements such as C_n^2 and l_o, as well as to quantify the propagation of uncertainty from source measurements to the calculated values of H_S and τ. Another type of turbulent flux is the latent heat flux H_L. The turbulent fluxes are given by

$$H_S = -\rho c_p u_\star T_\star, \tag{2.1}$$

$$H_L = -L_v u_\star q_\star, \tag{2.2}$$

$$\tau = \rho {u_\star}^2, \tag{2.3}$$

where $T_\star$ and $q_\star$ are the temperature and humidity scales, $u_\star$ is the friction velocity, ρ is the density of the air, c_p is the specific heat at constant pressure, and L_v is the latent heat

of vaporization. Determining area-averaged turbulent fluxes involves solving for $T_\star$ and $q_\star$, which are related to the path-length scale structure-function measurements through the non-linearly coupled Monin-Obukhov similarity equations [*Sorbjan*, 1989]. This procedure also involves solving for $u_\star$ in Eqs. 2.1, 2.2 and 2.3. The friction velocity $u_\star$ can be related either to path-length scale l_o measurements as with displaced-beam scintillometer strategies described in *Andreas* [1992], or to the wind profile and roughness length with large-aperture scintillometer strategies via the Businger-Dyer relation [*Panofsky and Dutton*, 1984; *Sorbjan*, 1989; *Lagouarde et al.*, 2002; *Hartogensis et al.*, 2003].

We consider here a displaced-beam scintillometer strategy in which path-averaged measurements of C_n^2 and l_o are obtained. Other required measurements include temporally-averaged pressure p, temperature T, humidity q, as well as the height of the beam above the underlying terrain z. Thus C_n^2, l_o, p, T, q and z are referred to as the source measurements. Each of these measurements demonstrates temporal and spacial variability as well as measurement uncertainty. Uncertainty propagates from the source measurements to the derived variables via the set of equations being considered. Uncertainties in l_o and C_n^2 are described in *Hill* [1988], while uncertainties in p, T and q depend on the particular instrument being used. Here, we explore the use of scintillometers over flat and homogeneous terrain, thus the height of the beam z is considered to be a single value with its associated uncertainty. While C_n^2 and l_o are representative of turbulent fluctuations along the whole beam, p, T and q are typically point measurements representative of localized areas near their respective instruments.

Applications for scintillometers include agricultural scientific studies such as *Hoedjes et al.* [2002] and *Foken et al.* [2008], and aggregation of surface measurements to satellite-retrieval scales for weather prediction and climate monitoring as in *Beyrich et al.* [2002] and in *Marx et al.* [2008]. The unique spacial scale of scintillometer measurements gives them the potential for a key role in bridging the gap between ground-based instruments with footprints on the order of 100 m^2 and model and satellite-retrieval scales on the order of 1 km^2.

The scale of scintillometer measurements introduces an additional complexity in the retrieval of the turbulent fluxes. This retrieval combines the large-scale scintillometer measured variables C_n^2 and l_o with source measurements that are not necessarily representative of the same scale. The only exception to be considered is the atmospheric pressure p. In particular, measurements of T and q may be representative of smaller footprints around their respective instruments. Specifically, assuming that variables such as average temperature T represent the entire beam path introduces a form of uncertainty. This uncertainty is somewhat similar to a systematic error, although it may be difficult to quantify because of its temporal variability.

Of previous scintillometer sensitivity studies, some stand out as possibly contradicting each other. For instance, the conclusion of the error analysis in *Moroni et al.* [1990] for a l_o and C_n^2 strategy was that *"The Monte Carlo analysis of the propagation of the statistical errors shows that there is only moderate sensitivity of the flux calculations to the initial errors in the measured quantities."* The error analysis of *Andreas* [1992], however, results in sensitivity functions that feature singularities. The sensitivity functions presented there imply that the resolution of $u_\star$ and consequently of H_S, H_L and τ by scintillometer l_o and C_n^2 measurements is intrinsically restricted to low precision over a certain range of environmental conditions. While these two studies use different methods and present results over slightly different ranges in variables, they produce sensitivity functions that for the same range differ significantly.

In Sect. 2.2 below, we decouple the set of equations including those of the Monin-Obukhov similarity hypothesis for l_o and C_n^2 scintillometer strategies for the example of unstable surface-layer conditions to arrive at single equations in single unknowns. The variable inter-dependency is mapped out as illustrated by tree diagrams. In Sect. 2.3, we take advantage of the mapped out variable inter-dependency to guide us in using the chain rule to solve the global partial derivatives in sensitivity functions to investigate error propagation. We produce sensitivity functions for H_S, τ and $u_\star$ as functions of both

l_o and z. In Sect. 2.4 we explore the ramifications of our results and compare them to previous literature, and we give conclusions in Sect. 2.5.

2.2 Measurement Strategy Case Study: Displaced-Beam Scintillometer System in Unstable Conditions

We consider here a two-wavelength system as introduced in *Andreas* [1989], where one of the scintillometers measures both l_o and C_n^2 as in *Andreas* [1992]. With this strategy, our measurements can resolve humidity and temperature fluctuations separately since the two scintillometers have different wavelengths λ_1 and λ_2 that have differing sensitivities in the index of refraction to humidity and temperature. This technique therefore requires fewer assumptions than the corresponding single-wavelength strategies as seen in *Andreas* [1989].

The following set of equations determines $T_\star$, $q_\star$ and $u_\star$ from the source measurements, and subsequently determines the turbulent fluxes:

$$\rho = \frac{p}{RT}, \tag{2.4}$$

$$l_o = \frac{(9\Gamma(1/3)KD(\rho,T))^{3/4}}{\varepsilon^{1/4}}, \tag{2.5}$$

$$\zeta = \frac{zg\kappa}{{u_\star}^2 T}\left(T_\star + \frac{0.61T}{\rho + 0.61q}q_\star\right), \tag{2.6}$$

$${u_\star}^3 = \frac{\kappa z\varepsilon}{\phi(\zeta)}, \tag{2.7}$$

$$C_{n_1}^2 = z^{-2/3}g(\zeta)(A_1(\lambda_1,p,T,q)T_\star + B_1(\lambda_1,p,T,q)q_\star)^2, \tag{2.8}$$

$$C_{n_2}^2 = z^{-2/3}g(\zeta)(A_2(\lambda_2,p,T,q)T_\star + B_2(\lambda_2,p,T,q)q_\star)^2, \tag{2.9}$$

where g is the local acceleration due to gravity, Γ is the Gamma function, ε is the turbulent energy dissipation rate, R is the specific gas constant, κ is the von Kármán constant, $\zeta \equiv z/L$, where L is the Obukhov length, K is the Obukhov-Corrsin constant, $\nu(T,\rho)$ is the viscosity of air and $D(T,\rho)$ is the thermal diffusivity of air (Andreas, 1989; 1992; 2012)

$C_{n_1}^2$ and $C_{n_2}^2$ are structure functions of the refractive index for the separate wavelengths λ_1 and λ_2. Eqs. 2.4 and 2.5 determine ε directly from l_o and the other source measurements. Inherent in Eqs. 2.8 and 2.9 is the assumption that $C_{Tq} = \sqrt{C_T^2 C_q^2}$, which is validated previously [*Hill*, 1989; *Andreas*, 1990].

The similarity functions $g(\zeta)$ and $\phi(\zeta)$ are given by

$$g(\zeta) = a(1 - b\zeta)^{-2/3}, \tag{2.10}$$

$$\phi(\zeta) = (1 + d(-\zeta)^{2/3})^{3/2}, \tag{2.11}$$

for $L < 0$ which corresponds to unstable conditions. The form of the similarity functions and their parameters follow from *Wyngaard et al.* [1971] and *Wyngaard and Coté* [1971]; the values are taken to be $a = 4.9$, $b = 6.1$, and $d = 0.46$ [*Andreas*, 1988].

The source measurements may not determine the sign of L, which is unknown a priori for every set of source measurements at any one time interval. We follow *Andreas* [1989] in solving for $T_\star$ and $q_\star$ from Eqs. 2.8 and 2.9, making sure to note that the signs of $\left(A_{1,2}T_\star + B_{1,2}q_\star\right)$ are not yet solved by introducing unknowns sign_1 and sign_2:

$$\frac{\text{sign}_1\sqrt{C_{n_1}^2}z^{1/3}(1 - b\zeta)^{1/3}}{\sqrt{a}} = A_1 T_\star \left(1 + \frac{B_1}{A_1}\frac{q_\star}{T_\star}\right), \tag{2.12}$$

$$\frac{\text{sign}_2\sqrt{C_{n_2}^2}z^{1/3}(1 - b\zeta)^{1/3}}{\sqrt{a}} = A_2 T_\star \left(1 + \frac{B_2}{A_2}\frac{q_\star}{T_\star}\right), \tag{2.13}$$

where the roots on the left-hand side are considered to be positive. Following *Andreas* [1989], these can be re-arranged to isolate $T_\star$ and $q_\star$ with the as yet undetermined signs:

$$T_\star = \frac{(1-b\zeta)^{1/3}z^{1/3}}{\sqrt{a}}\left(\frac{\mathrm{sign}_1\sqrt{C_{n_1}^2}B_2 - \mathrm{sign}_2\sqrt{C_{n_2}^2}B_1}{A_1B_2 - A_2B_1}\right), \tag{2.14}$$

$$q_\star = \frac{(1-b\zeta)^{1/3}z^{1/3}}{\sqrt{a}}\left(\frac{\mathrm{sign}_2\sqrt{C_{n_2}^2}A_1 - \mathrm{sign}_1\sqrt{C_{n_1}^2}A_2}{A_1B_2 - A_2B_1}\right), \tag{2.15}$$

where

$$\mathrm{sign}_{1,2} = \mathrm{sign}[A_{1,2}T_\star(1 + \frac{B_{1,2}}{A_{1,2}}\frac{q_\star}{T_\star})]. \tag{2.16}$$

It is useful to include the definition of the Bowen ratio as

$$\beta \equiv H_S/H_L = \frac{\rho c_p}{L_v}\frac{T_\star}{q_\star}. \tag{2.17}$$

We can solve for β as

$$\beta = E\left(\frac{\mathrm{sign}_1\sqrt{C_{n_1}^2}B_2 - \mathrm{sign}_2\sqrt{C_{n_2}^2}B_1}{\mathrm{sign}_2\sqrt{C_{n_2}^2}A_1 - \mathrm{sign}_1\sqrt{C_{n_1}^2}A_2}\right), \tag{2.18}$$

where $E(T,p) = \rho c_p/L_v$. It is useful to consider β as well as ζ as unit-less independent variables in our sensitivity analyses that represent certain meteorological regimes. They represent the ratio of the sensible to latent heat fluxes and an indicator of surface-layer stability, respectively.

Since we are considering unstable conditions, we have $\zeta < 0$ since $L < 0$, so from Eq. 2.6 we have

$$T_\star(1+\frac{0.61T}{\rho+0.61q}\frac{q_\star}{T_\star})<0, \tag{2.19}$$

$$(1-b\zeta)>0, \tag{2.20}$$

$$(1+d(-\zeta)^{2/3})^{3/2}>0, \tag{2.21}$$

We begin decoupling the set of equations by taking Eqs. 2.14 and 2.15 and substituting into Eq. 2.6, then cubing the resulting equation as well as squaring Eq. 2.7 to arrive at

$$\zeta^3 = \frac{z^4 g^3 \kappa^3 (1-b\zeta)}{{u_\star}^6 T^3 a^{3/2}}\left[F^3(1+H/\beta)^3\right], \tag{2.22}$$

$${u_\star}^6 = \frac{\kappa^2 z^2 \varepsilon^2}{(1+d(-\zeta)^{2/3})^3}, \tag{2.23}$$

where $F(T,p,q,\lambda_1,\lambda_2,C_{n_1}^2,C_{n_2}^2)$ and $H(T,p,q)$ are defined as

$$F(T,p,q,\lambda_1,\lambda_2,C_{n_1}^2,C_{n_2}^2) = \frac{\mathrm{sign}_1\sqrt{C_{n_1}^2}B_2-\mathrm{sign}_2\sqrt{C_{n_2}^2}B_1}{A_1B_2-A_2B_1}, \tag{2.24}$$

$$H(T,p,q) = E\left(\frac{0.61T}{\rho+0.61q}\right). \tag{2.25}$$

We then combine Eqs. 2.22 and 2.23 to obtain a final equation in ζ:

$$\zeta^3 = M(1-b\zeta)(1+d(-\zeta)^{2/3})^3, \tag{2.26}$$

where

$$M \equiv \frac{g^3 z^2 \kappa[F^3(1+H/\beta)^3]}{T^3 \varepsilon^2 a^{3/2}}, \tag{2.27}$$

is determined directly from the source measurements. Here we note that the left-hand side is negative, and so the term in square brackets in M is negative as well. From any set of measurements we know the sign of $A_1B_2-A_2B_1$, and we also know the values of

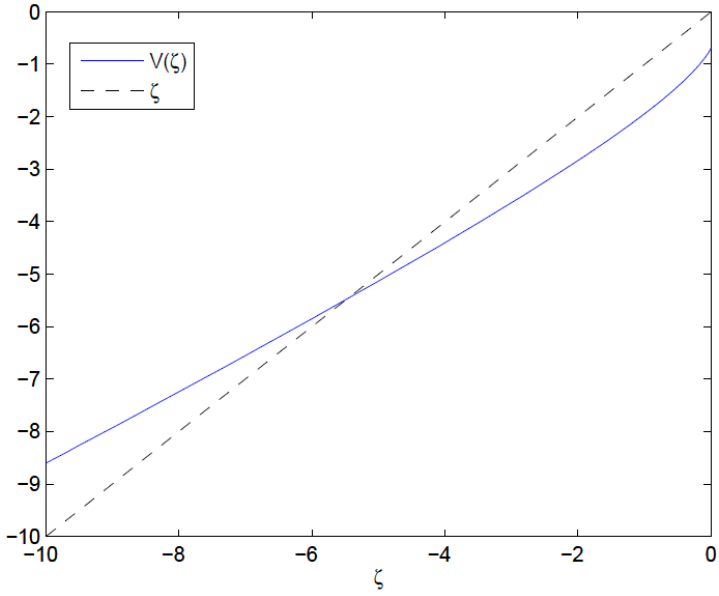

Figure 2.1. Visualization of the solution of Eq. 2.26 using fixed-point recursion, with $M = -1/3$. The function $\zeta = V(\zeta)$ is used, where $V(\zeta) \equiv M^{1/3}(1 - b\zeta)^{1/3}(1 + d(-\zeta)^{2/3})$. Real roots of $M^{1/3}$ are chosen. The recursive series $[V(\zeta_{guess}), V(V(\zeta_{guess})), V(V(V(\zeta_{guess}))), V(V(V(V(\zeta_{guess}))))...]$ converges for any $\zeta_{guess} < 0$.

the two terms that multiply the unknown signs. Occasionally these relations are enough to determine all the signs; otherwise the signs remain ambiguous and they are evaluated from observations of the temperature and humidity stratification as seen in *Andreas* [1989].

140

Eq. 2.26 can be solved with a fixed-point recursive technique as illustrated in Fig. 2.1. The recursive function

$$\zeta = V(\zeta) \equiv M^{1/3}(1 - b\zeta)^{1/3}(1 + d(-\zeta)^{2/3}) \tag{2.28}$$

is used. A solution of Eq. 2.26 using fixed-point recursion is seen in Fig. 2.2.

145 A good estimate of the uncertainty in the derived variables that results from small errors in source measurements is given by

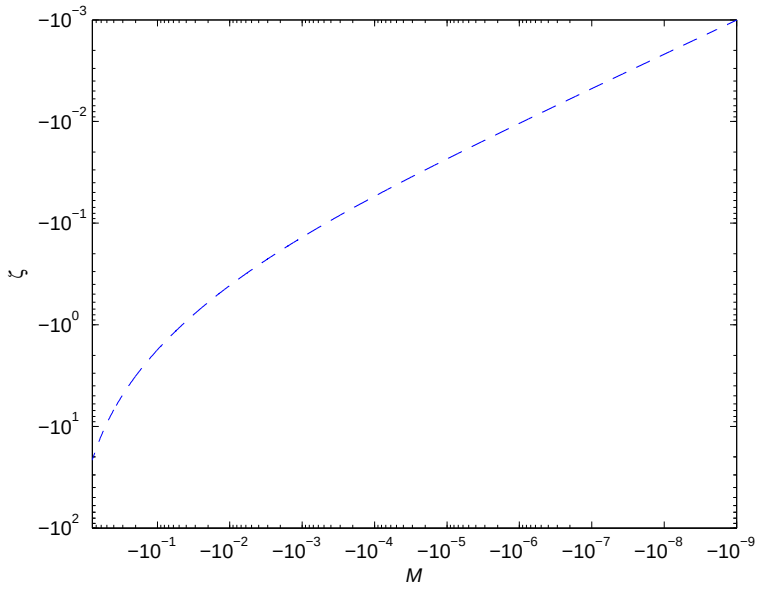

Figure 2.2. Solution of Eq. 2.26 using fixed-point recursion on the function $\zeta = V(\zeta)$ where $V(\zeta) \equiv M^{1/3}(1 - b\zeta)^{1/3}(1 + d(-\zeta)^{2/3})$. Real roots of $M^{1/3}$ are chosen. Note that for $M = -1/3$, we have $\zeta \approx -5.5$ as in Fig. 2.1. Computational error was verified to be completely negligible with minimal running time involved.

$$\sigma_f = \sum_{i=1}^{N} \left(\frac{\partial f}{\partial x_i} \right) \sigma_{x_{s_i}} + \sqrt{\sum_{i=1}^{N} \left(\frac{\partial f}{\partial x_i} \right)^2 \sigma^2{}_{x_{r_i}}} + \sigma_{f_c}, \tag{2.29}$$

where the derived variable f is a function of source measurement variables $x_1, x_2, ..., x_N$ with respective systematic error $\sigma_{x_{s_1}}, \sigma_{x_{s_2}}, ..., \sigma_{x_{s_N}}$ and with respective independent Gaussian distributed uncertainties with standard deviations $\sigma_{x_{r_1}}, \sigma_{x_{r_2}}, ..., \sigma_{x_{r_N}}$ as seen in *Taylor* [1997]. The numerical indices indicate different independent variables, such as T, p, or z, for example. Computational error f due to the inaccurate solution of the theoretical equations is represented by σ_{f_c}. The first and last terms in Eq. 2.29 represent an offset from the true solution (inaccuracy), whereas the central square-root term represents the breadth of uncertainty due to random error (imprecision).

It is practical for the purpose of a sensitivity study to rewrite Eq. 2.29 as

$$\frac{\sigma_f}{f} = \sum_{i=1}^{N} S_{f,x} \frac{\sigma_{x_{s_i}}}{x_{s_i}} + \sqrt{\sum_{i=1}^{N} S_{f,x}^2 \frac{\sigma^2{}_{x_{r_i}}}{x_{r_i}{}^2}} + \frac{\sigma_{f_c}}{f}, \tag{2.30}$$

where $S_{f,x}$ are unitless sensitivity functions defined by

$$S_{f,x} \equiv \frac{x}{f} \left(\frac{\partial f}{\partial x} \right). \tag{2.31}$$

The sensitivity functions are each a measure of the portion of the error in the derived variable f resulting from error on each individual source measurement x. In addition to the error on source measurement variables, we can also recognize that a, b and d have been resolved to some level of certainty by fitting field data. We thus treat them here in the same way as source measurements.

In the application of Eqs. 2.29 and 2.30, we recognize the addition of the computational error σ_{f_c}. In previous field and sensitivity studies [*Lagouarde et al.*, 2002; *de Bruin et al.*, 2002; *Solignac et al.*, 2009; *Andreas*, 2012], the full set of equations has been incorporated into a cyclically iterative algorithm which cycles through the full set of equations,

allowing multiple variables to change. This numerical algorithm sometimes fails to converge, as demonstrated in *Andreas* [2012].

The problem of resolving the uncertainty on the derived variables is a matter of identifying the magnitude and character of the source measurement uncertainties, and then solving for the partial derivative terms in Eqs. 2.29 and 2.31. These derivatives are global[2] ; that is, they take into account all the relationships in all of the relevant equations through which the variable f is derived. Without an analytic solution of the set of coupled equations we could either solve for the partial derivatives through a total-differential expansion of each equation individually, followed by a re-grouping of all differential terms as seen in Andreas (1989; 1992) or we could use numerical error propagation techniques as in the Monte Carlo analysis of *Moroni et al.* [1990] or as in the analysis of *Solignac et al.* [2009].

We investigate inter-variable sensitivity analytically via Eq. 2.31, using Eq. 2.26 as a starting point. We use Eq. 2.26 to determine the details of the variable inter-dependency to define our use of the chain rule. A tree diagram representing the variable inter-dependency is broken into three parts shown in Figs. 2.3, 2.4, and 2.5.

Eq. 2.26 can be reduced to a choice of two algebraic equations

$$\alpha > 0, -\alpha^9 = M(1+d\alpha^2)^3(1+b\alpha^3), \zeta = -\alpha^3, \frac{\partial \zeta}{\partial \alpha} = -3\alpha^2 < 0, \tag{2.32}$$

$$\alpha < 0, \alpha^9 = M(1+d\alpha^2)^3(1-b\alpha^3), \zeta = \alpha^3, \frac{\partial \zeta}{\partial \alpha} = 3\alpha^2 > 0, \tag{2.33}$$

[2]Global partial derivatives are those which propagate from the dependent (derived) variable down to the independent (source measurement) variable through the entire tree diagram, whereas local partial derivatives propagate as if the equation being differentiated were independent of the rest of the equations in the set. An alternative to direct evaluation of global partial derivatives via the chain rule is a total-differential expansion (where all derivatives are local) of each equation in the set. This approach can be used to solve for global partial derivatives by re-grouping all total-differential terms into one equation. Readers may refer to *Sokolnikoff* [1939].

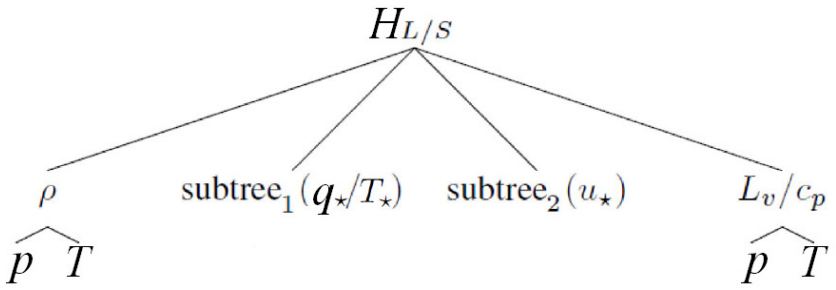

Figure 2.3. Variable inter-dependency tree diagram for a two-wavelength measurement strategy inferring $H_{L/S}$ through path-averaged $u_\star$ and $q_\star/T_\star$ measurements via scintillometer measurements of l_o and C_n^2 under unstable meteorological conditions ($\zeta < 0$). Variables at the bottom of the tree are source measurements; all others are considered to be derived variables. The "/" symbol is meant to delineate between two independent tree diagrams. Note that H_L is not a direct function of ρ; this branch is for the convenience of including H_S since the rest of their tree diagrams are identical. Figs. 2.4 and 2.5 feature subtree$_1$ and subtree$_2$, respectively.

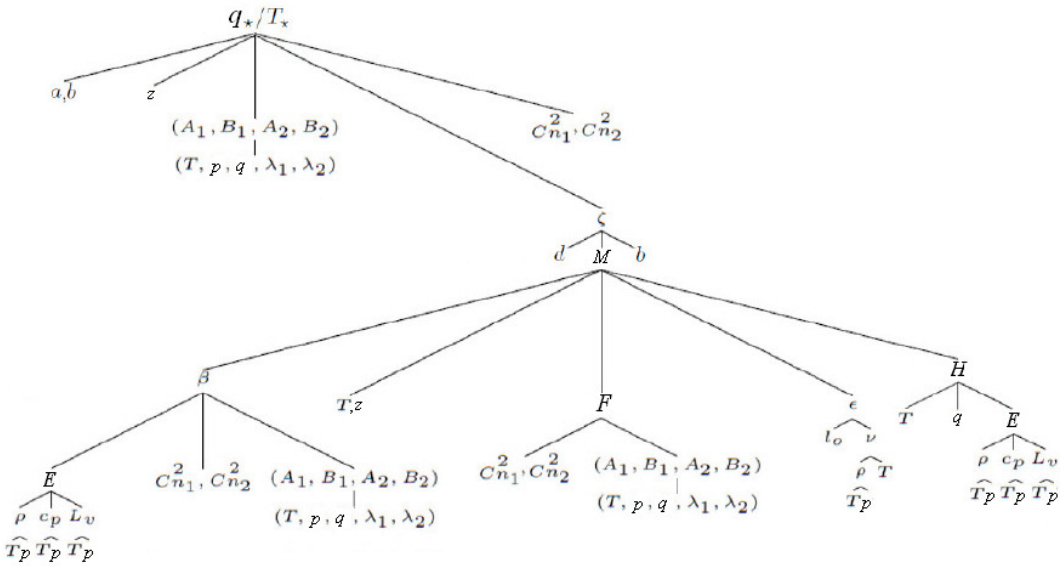

Figure 2.4. Subtree$_1$ of variable inter-dependency for $\zeta < 0$. The main tree diagram is seen in Fig. 2.3.

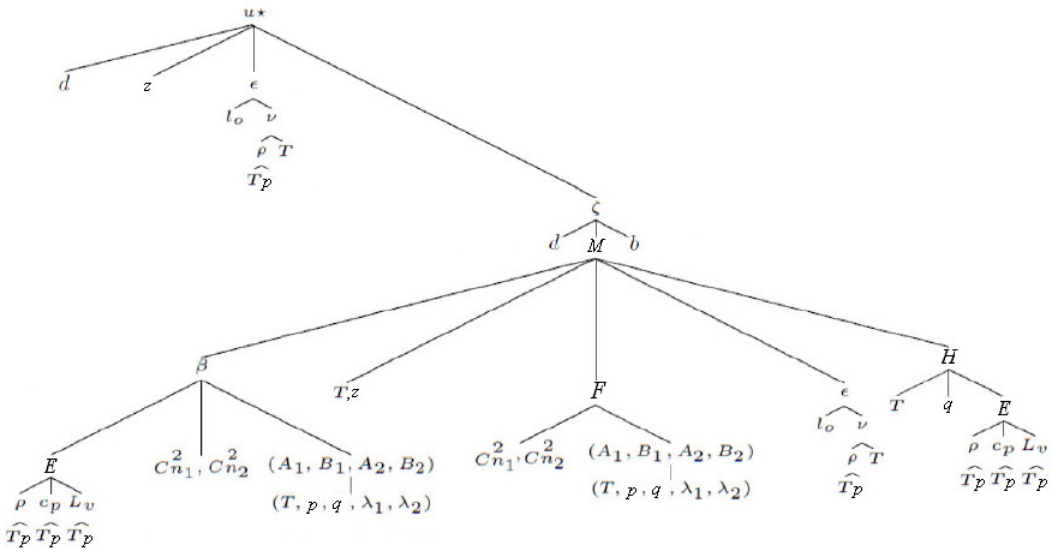

Figure 2.5. Subtree$_2$ of variable inter-dependency for $\zeta < 0$. The main tree diagram is seen in Fig. 2.3.

with the substitution

$$\alpha^2 \equiv (-\zeta)^{2/3} > 0. \tag{2.34}$$

Galois theory implies that, since Eqs. 2.32 and 2.33 are ninth order, there is no way to write $\zeta = f(p, T, q, C_{n_1}^2, C_{n_2}^2, \lambda_1, \lambda_2, z, l_o)$ for any general values of b and d, where f is an explicit function of the source measurements [*Edwards*, 1984]. It is thus simplest to extract $\left(\frac{\partial \zeta}{\partial M}\right)$ by implicit differentiation of Eq. 2.26; the results are in given in Appendix 2.A.

2.3 Results: Derivation of Sensitivity Functions

Following the solution method described above, we solve for global partial derivative terms in Eqs. 2.29 and 2.31 through use of the general chain rule guided by the variable inter-dependency tree diagrams seen in Figs. 2.3, 2.4 and 2.5. We will obtain sensitivity functions of the sensible heat flux H_S and the momentum flux τ as functions of z and ε. From Eqs. 2.1, 2.5 and 2.31 we have

$$S_{H_S,\varepsilon} = S_{T_\star,\varepsilon} + S_{u_\star,\varepsilon} = -\frac{1}{4} S_{H_S,l_o}, \tag{2.35}$$

$$S_{H_S,z} = S_{T_\star,z} + S_{u_\star,z}, \tag{2.36}$$

and from Eqs. 2.3, 2.5 and 2.31, we have

$$S_{\tau,\varepsilon} = 2S_{u_\star,\varepsilon} = -\frac{1}{4} S_{\tau,l_o}, \tag{2.37}$$

$$S_{\tau,z} = 2S_{u_\star,z}, \tag{2.38}$$

thus we seek solutions for $S_{T_\star,z}$, $S_{u_\star,z}$, $S_{T_\star,\varepsilon}$, and $S_{u_\star,\varepsilon}$.

We first obtain $S_{T_\star,\varepsilon}$ with guidance from the tree diagram depicted in Fig. 2.4:

$$S_{T_\star,\varepsilon} = \frac{\varepsilon}{T_\star}\left(\frac{\partial T_\star}{\partial \zeta}\right)\left(\frac{\partial \zeta}{\partial M}\right)\left(\frac{\partial M}{\partial \varepsilon}\right). \tag{2.39}$$

The individual terms of Eq. 2.39 are given in Appendices 2.A and 2.B. Combining them, we obtain

$$S_{T_\star,\varepsilon} = \frac{1}{3}\left(\frac{2b\zeta(-\zeta)^{1/3}(1+d(-\zeta)^{2/3})}{(3-2b\zeta)(1+d(-\zeta)^{2/3})(-\zeta)^{1/3}+2d\zeta(1-b\zeta)}\right). \tag{2.40}$$

We now obtain $S_{T_\star,z}$:

$$S_{T_\star,z} = \frac{z}{T_\star}\left[\left(\frac{\partial T_\star}{\partial z}\right)_\zeta + \left(\frac{\partial T_\star}{\partial \zeta}\right)_z \left(\frac{\partial \zeta}{\partial M}\right)\left(\frac{\partial M}{\partial z}\right)\right]. \tag{2.41}$$

The individual terms of Eq. 2.41 are developed in Appendices 2.A and 2.C. Combining them, we obtain

$$S_{T_\star,z} = \frac{1}{3}\left[1 - \left(\frac{2b\zeta(-\zeta)^{1/3}(1+d(-\zeta)^{2/3})}{(3-2b\zeta)(1+d(-\zeta)^{2/3})(-\zeta)^{1/3}+2d\zeta(1-b\zeta)}\right)\right]. \tag{2.42}$$

We now obtain $S_{u_\star,\varepsilon}$ with guidance from the tree diagram depicted in Fig. 2.5. We have

$$S_{u_\star,\varepsilon} = \frac{\varepsilon}{u_\star}\left[\left(\frac{\partial u_\star}{\partial \varepsilon}\right)_\zeta + \left(\frac{\partial u_\star}{\partial \zeta}\right)_\varepsilon \left(\frac{\partial \zeta}{\partial M}\right)\left(\frac{\partial M}{\partial \varepsilon}\right)\right]. \tag{2.43}$$

The individual terms in Eq. 2.43 are developed in Appendices 2.A and 2.D. Combining them, we obtain

$$S_{u_\star,\varepsilon} = \frac{1}{3}\left[1 - \left(\frac{2d\zeta(1-b\zeta)}{(3-2b\zeta)(1+d(-\zeta)^{2/3})(-\zeta)^{1/3}+2d\zeta(1-b\zeta)}\right)\right]. \tag{2.44}$$

We now obtain $S_{u_\star,z}$. We have

$$S_{u_\star,z} = \frac{z}{u_\star}\left[\left(\frac{\partial u_\star}{\partial z}\right)_\zeta + \left(\frac{\partial u_\star}{\partial \zeta}\right)_z \left(\frac{\partial \zeta}{\partial M}\right)\left(\frac{\partial M}{\partial z}\right)\right]. \tag{2.45}$$

The individual terms in Eq. 2.45 are developed in Appendices 2.A and 2.E. Combining them we obtain

$$S_{u_\star,z} = \frac{1}{3}\left[1 + \left(\frac{2d\zeta(1-b\zeta)}{(3-2b\zeta)(1+d(-\zeta)^{2/3})(-\zeta)^{1/3}+2d\zeta(1-b\zeta)}\right)\right]. \tag{2.46}$$

Combining our results in Eqs. 2.39, 2.41, 2.43, and 2.45, we can obtain $S_{H_S,\varepsilon}$ and $S_{H_S,z}$ from Eqs. 2.35 and 2.36; the results are seen in Fig. 2.6.

The absolute value of our results for S_{H_S,l_o} given by Eqs. 2.35, 2.40 and 2.44 is similar to the sensitivity multiplier found in *Moroni et al.* [1990] as seen in their Fig. 10. The absolute value of our result of S_{τ,l_o} given by Eqs. 2.37 and 2.44 is also compatible with the results of *Moroni et al.* [1990] seen in their Fig. 9. However, our result for $S_{u_\star,\varepsilon}$ in Eq. 2.44 differs from that obtained in *Andreas* [1992] as seen in Fig. 2.7. Similarly, our result for $S_{u_\star,z}$ in Eq. 2.46 differs from that obtained in *Andreas* [1992] as seen in Fig. 2.8.

2.4 Discussion

The reason for the difference between our results and those of *Andreas* [1992] in Figs. 2.7 and 2.8 can be seen to have arisen in Eqs. A.7 and A.10 of *Andreas* [1992] . Even though

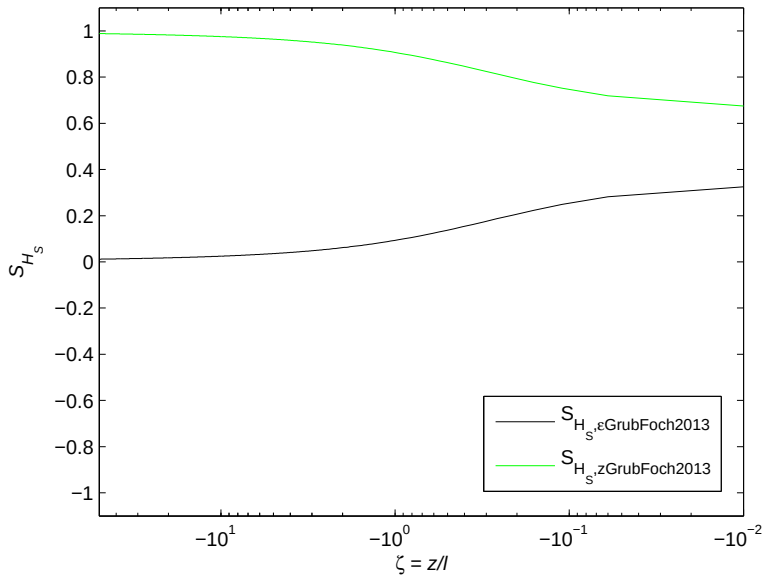

Figure 2.6. Sensitivity functions for H_S with regards to measurements of ε and z in the path-averaged $u_\star$ scintillation measurement, for unstable conditions corresponding to $\zeta < 0$.

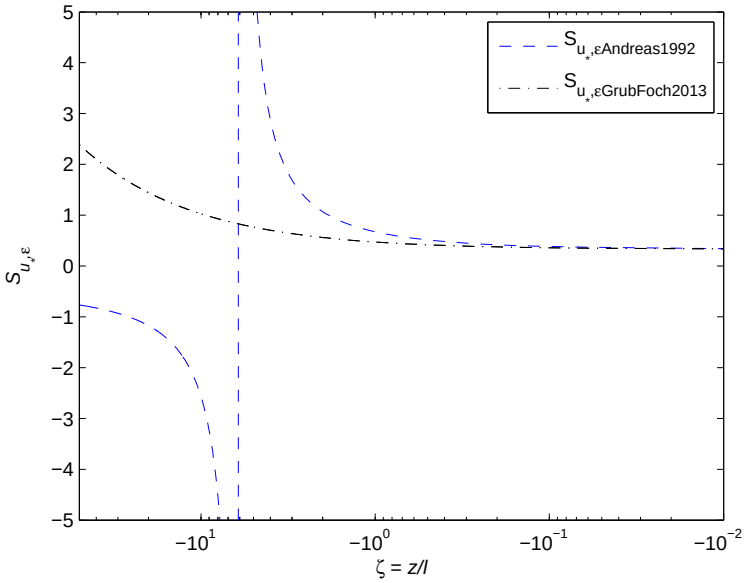

Figure 2.7. Sensitivity function for $u_\star$ with regards to measurements of ε in the path-averaged $u_\star$ scintillation measurement. Results from *Andreas* [1992] are plotted (denoted there as S_ε) along with Eq. 2.44 derived here for $\zeta < 0$.

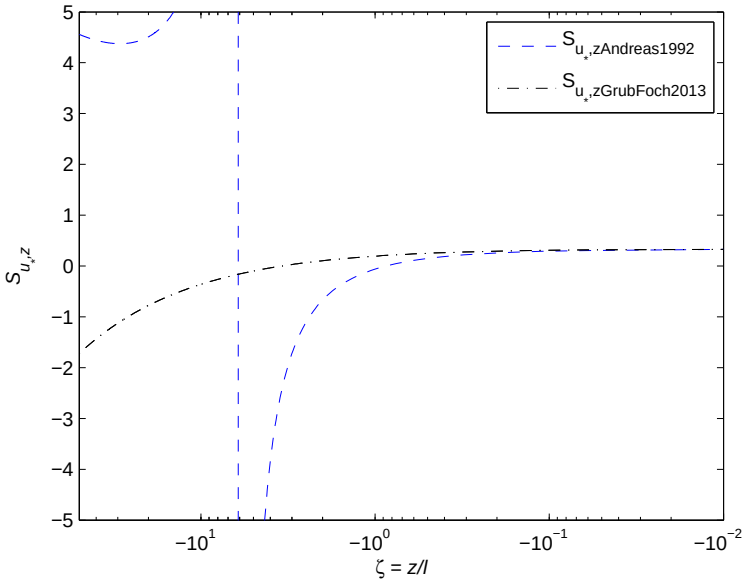

Figure 2.8. Sensitivity function for $u_\star$ with regards to measurements of z in the path-averaged $u_\star$ scintillation measurement. Results from *Andreas* [1992] are plotted (denoted there as S_{zz}) along with Eq. 2.46 derived here for $\zeta < 0$.

there is a typographical error in Eq. A.7 in the application of the product rule (it should be

$$\frac{\partial \varepsilon}{\partial u_\star} = \frac{3{u_\star}^2}{\kappa z}\phi_\varepsilon(\zeta) + \frac{{u_\star}^3}{z\kappa}\frac{\partial \phi_\varepsilon}{\partial \zeta}\frac{\partial \zeta}{\partial u_\star}, \tag{2.47}$$

where the second term contained $u_\star^2$ originally), this is not the origin of the reason since the result in Eq. A.8 follows from the modified Eq. A.7. The reason is found to be that
230 Eqs. A.7 and A.8 are not differentiated locally with respect to Eq. 1.3 of *Andreas* [1992] as they should be in a total-differential expansion. The local derivative is

$$\frac{\partial \varepsilon}{\partial u_\star} = \frac{\partial}{\partial u_\star}\left(\frac{u_\star^3}{\kappa z}\phi_\varepsilon(\zeta)\right) = \frac{3{u_\star}^2}{\kappa z}\phi_\varepsilon(\zeta) = \frac{3\varepsilon}{u_\star}, \tag{2.48}$$

keeping ζ constant regardless of the relationship between ζ and $u_\star$. The relationship between ζ and $u_\star$ is taken into account when we re-group the full set of locally expanded equations (which are coupled in ζ and $u_\star$). The second term on the right-hand side of Eq.
235 2.47 and Eq. A.7 of *Andreas* [1992] is thus not necessary and does not appear in Eq. 2.48. Taking into account the relationship between ζ and $u_\star$ via the chain rule is appropriate for direct evaluation of global derivatives, but not in individual derivatives of a total-differential expansion of the full set of equations. Eqs. A.10 and A.11 of *Andreas* [1992] have the same issues of not being differentiated locally with respect to Eq. 1.3 of *Andreas*
240 [1992]. The local derivative there is

$$\frac{\partial \varepsilon}{\partial z} = -\frac{\varepsilon}{z}. \tag{2.49}$$

A re-analysis of the *Andreas* [1992] differential expansion including the local derivatives in Eqs. 2.48 and 2.49 is reproduced in Appendix 2.F; the results for $S_{u_\star,\varepsilon}$ and $S_{u_\star,z}$ are identical to those found here in Eqs. 2.43 and 2.45. Note that the left-hand side of Eq. 2.89 contains the terms $(S_{u_\star} - 2)$ and $(S_z + 1)$ instead of $(S_{u_\star} - 4)$ and $(S_z + 2)$ as in Eq. A.16 of
245 *Andreas* [1992]. These differences also influence the *Andreas* [1992] sensitivity functions for C_{n1}^2 and C_{n2}^2.

The technique presented here for the direct evaluation of partial derivatives can be applied to evaluate sensitivity functions for other variables involved in this scintillometer strategy for both stable and unstable conditions, however we will now focus on the implications of our results on other previous studies. Another instance where we found divergence in results is in the study of *Hartogensis et al.* [2003] where $S_{H_S,z}$ in Eq. A2 and Fig. A1 should be the same as the results of *Andreas* [1989] in Fig. 4, regardless of the differences between a single and double wavelength strategy. Note that in *Andreas* [1989], for $\zeta = 0$, it was found that

$$S_{H_S,z}(0) = S_{T_\star,z}(0) = 1/3, \tag{2.50}$$

for a scintillometer strategy involving independent $u_\star$ measurements, whereas a value of $1/2$ was found in *Hartogensis et al.* [2003]. The issue here is not due to the differences in scintillation strategies (note that the Businger-Dyer relation is ignored in the sensitivity study of *Hartogensis et al.* [2003]). The issue is that Eq. A1 of *Hartogensis et al.* [2003] is coupled to Eqs. 5-6 of *Hartogensis et al.* [2003] in L. In the derivation of Eq. A1, *Hartogensis et al.* [2003] essentially have considered Z_{LAS} to be the same z as in *Andreas* [1989], and they have considered similar equations that assume an independent $u_\star$ measurement (Eq. 7 of *Hartogensis et al.* [2003] is ignored). Including the coupling of Eq. 7 of *Hartogensis et al.* [2003] (the Businger-Dyer relation) in L adds complication; however if we continue to assume an independent $u_\star$ measurement, we achieve the same results as in *Andreas* [1989], viz:

$$S_{H_S,z} = S_{T_\star,z} = \frac{1-2b\zeta}{3-2b\zeta} \neq \frac{1-2b\zeta}{2-2b\zeta} = \frac{z}{H_S}\left(\frac{\partial H_S}{\partial z}\right)_L. \tag{2.51}$$

A similar example is in the analysis of *Hartogensis et al.* [2002], when the sensitivity of $u_\star$ to l_o is being examined. Eq. 13 of *Hartogensis et al.* [2002] is not a "direct" relation of $u_\star$ to source measurements, since L is a derived variable. There is coupling to L and thus we may investigate the sensitivity with

$$\left(\frac{\partial u_\star}{\partial l_o}\right) = \left(\left(\frac{\partial u_\star}{\partial \varepsilon}\right)_\zeta + \left(\frac{\partial u_\star}{\partial \zeta}\right)\left(\frac{\partial \zeta}{\partial M}\right)\left(\frac{\partial M}{\partial \varepsilon}\right)\right)\left(\frac{\partial \varepsilon}{\partial l_0}\right), \tag{2.52}$$

where M is modified for the single scintillometer l_o and C_n^2 strategy. Also in *Hartogensis et al.* [2002], it is stated that errors in C_T^2 are attenuated in deriving $\theta_\star$ (here denoted $T_\star$) due to the square-root dependence; however we can go a step further by realizing that Eq. 9 of *Hartogensis et al.* [2002] is not yet decoupled from L. As follows from our analysis applied to the case considered in *Hartogensis et al.* [2002] (modifying Fig. 2.4 for a single-wavelength strategy), we obtain

$$\left(\frac{\partial T_\star}{\partial C_T^2}\right) = \left(\frac{\partial T_\star}{\partial C_T^2}\right)_\zeta + \left(\frac{\partial T_\star}{\partial \zeta}\right)\left(\frac{\partial \zeta}{\partial M}\right)\left(\frac{\partial M}{\partial C_T^2}\right). \tag{2.53}$$

Note that there may be no way to actually obtain "direct" relationships between the source measurements and the derived variables if the implicit equation in ζ (such as Eq. 2.26) is fifth order or higher.

2.5 Conclusions

A new method of deriving sensitivity functions for l_o and C_n^2 scintillometer measurements of turbulent fluxes has been produced by mapping out the variable inter-dependency and solving for partial derivatives with the chain rule. We have bypassed the need for an explicit solution to the theoretical equations by including one implicit differentiation step on Eq. 2.26, which is a bottleneck on the tree diagrams seen in Figs. 2.4 and 2.5. This allows for the evaluation of sensitivity functions that are useful not only for optimizing the measurement strategy and selecting the most ideal wavelengths, but the closed, compact form of sensitivity functions produced using the method presented here is convenient to incorporate into computer code for the analysis of data. It is noteworthy that the actual functional relations change at $z/L = 0$, which corresponds to neutral conditions. Thus, for any set of source measurements we should calculate the set of all derived variables and their respective uncertainties assuming both stable and unstable conditions. If errors on

z/L overlap with $z/L = 0$ for either stability regime, we should then consider the combined range of errors.

In addition to the source measurements, the empirical parameters a, b and d have been included in the tree diagrams. Future study should quantify the sensitivity of derived variables to these parameters. In considering errors on the empirical parameters or on other source measurements such as T, a total-differential expansion such as in Andreas (1989; 1992) may become intractable, whereas an analysis of the type presented here remains compact.

Results obtained here have resolved some issues in the previous literature. For example, we have confirmed the conclusion of *Moroni et al.* [1990] that l_o and C_n^2 scintillometers can obtain fairly precise measurements of turbulent fluxes. In the range of $-1 \leq \zeta \leq -0.01$, the results derived here for $S_{u_\star,\varepsilon}$ and $S_{u_\star,z}$ are similar to those in *Andreas* [1992]; however for $\zeta < -1$ the separate results differ greatly in both magnitude and in the shape of the curves as seen in Figs. 2.7 and 2.8. These sensitivity functions in *Andreas* [1992] contain singularities near $\zeta \approx -6$; this effectively implies that it is impossible to resolve $u_\star$ in this stability regime. The sensitivity functions derived here demonstrate a small magnitude for typical values of ζ including the range $-10 < \zeta < -1$. The sensitivities of the sensible heat flux to uncertainties in ε and z are found in Eqs. 2.35 and 2.36 and are seen in Fig. 2.6; they are compatible with the results of *Moroni et al.* [1990] and they imply that, with optimal wavelengths, we can arrive at reasonably precise measurements of path-averaged turbulent fluxes and friction velocity.

An advantageous byproduct of having reduced the system of equations into a single equation in a single unknown is that the error in the actual computation of the derived variables can be essentially eliminated, or it can be estimated. Eqs. 2.32 and 2.33 are polynomials; numerical methods for their accurate solution are well established. Using fixed-point recursion, the maximum computational error can be resolved, and monotonic convergence can be guaranteed as seen in *Traub* [1964] and more recently in *Agarwal et al.*

[2001].

In contrast, the classical iterative algorithm (Andreas, 1989; 2012; Hartogensis, 2003; Solignac, 2009) may diverge or alternate about a potential solution. At worst, techniques such as the classical algorithm may stop at a "bottleneck" and converge to a false solution as illustrated in *Press et al.* [1992]. In their section on non-linear coupled equations, it is stated:

"We make an extreme, but wholly defensible, statement: there are no good, general (numerical) *methods for solving systems of more than one non-linear equation. Furthermore, it is not hard to see why (very likely), there never will be any good, general* (numerical) *methods..."*

In *Hill et al.* [1992], similar one-dimensional iterative methods of numerical computation of ζ were used to eliminate computational error, however the fixed-point algorithm we have presented converges for any ζ_{guess} (with the correct sign). We argue that at least some of the spread of data in Figs. 5 and 6 in *Andreas* [2012] may be due to computational uncertainty as well as the incorporation of $T_\star$, L, and $u_\star$ measured at the scale of an eddy covariance system's footprint while being forced to assume that they are representative of the beam path scale. The scatter in these plots may not be entirely due to unreliable l_o and C_n^2 measurements.

Future expansions of the sensitivity analysis presented here may focus on taking into account field sites with heterogeneous terrain and variable topography. For stationary turbulence with beams above the blending height, the line integral formulation for effective beam height given by Eq. B2 in *Hartogensis et al.* [2003] and Eqs. 10-12 in *Kleissl et al.* [2008] could be incorporated. Two-dimensional footprint analyses involving surface integrals that take into account variable roughness length and wind direction as in *Meijninger et al.* [2002] and in *Liu et al.* [2011] may be incorporated for flat terrain that is heterogeneous enough to force the scintillometer beam to be below the blending height [*Wieringa*, 1976; *Mason*, 1988]. Further theoretical developments may be anticipated that

take into account both heterogeneity and variable topography. It is hoped that the general mathematical approach presented here can help to keep track of uncertainty for any scintillometer application, as well as to eliminate the byproducts of iteration.

Acknowledgements

The authors thank the Geophysical Institute at the University of Alaska Fairbanks for its support, Derek Starkenburg and Peter Bieniek for assistance with editing, two anonymous reviewers, one in particular, for very helpful comments. In addition, the authors thank Flora Grabowska of the Mather library for her determination in securing funding for open access fees. GJ Fochesatto was partially supported by the Alaska Space Grant NASA-EPSCoR program award number NNX10N02A.

2.A Relations between M and ζ

$$M = \frac{\zeta^3}{(1+d(-\zeta)^{2/3})^3(1-b\zeta)}, \tag{2.54}$$

$$\left(\frac{\partial\zeta}{\partial M}\right) = \left(\frac{(1-b\zeta)(1+d(-\zeta)^{2/3})^3}{3\zeta^2+M[2d(1-b\zeta)(1+d(-\zeta)^{2/3})^2(-\zeta)^{-1/3}+b(1+d(-\zeta)^{2/3})^3]}\right), \tag{2.55}$$

$$M\left(\frac{\partial\zeta}{\partial M}\right) = \left(\frac{\zeta(1-b\zeta)(1+d(-\zeta)^{2/3})}{(3-2b\zeta)(1+d(-\zeta)^{2/3})+2d\zeta(-\zeta)^{-1/3}(1-b\zeta)}\right). \tag{2.56}$$

2.B Individual terms in $S_{T_\star,\varepsilon}$ for unstable conditions ($\zeta < 0$)

$$\left(\frac{\partial T_\star}{\partial\zeta}\right) = T_\star\left(\frac{-b}{3(1-b\zeta)}\right), \tag{2.57}$$

$$\left(\frac{\partial M}{\partial\varepsilon}\right) = -2M/\varepsilon. \tag{2.58}$$

2.C Individual terms in $S_{T_\star,z}$ for unstable conditions ($\zeta < 0$)

$$\left(\frac{\partial T_\star}{\partial z}\right)_\zeta = \frac{T_\star}{3z}, \tag{2.59}$$

$$\left(\frac{\partial T_\star}{\partial \zeta}\right)_z = T_\star\left(\frac{-b}{3(1-b\zeta)}\right), \tag{2.60}$$

$$\left(\frac{\partial M}{\partial z}\right) = 2M/z. \tag{2.61}$$

2.D Individual terms in $S_{u_\star,\varepsilon}$ for unstable conditions ($\zeta < 0$)

$$\left(\frac{\partial u_\star}{\partial \varepsilon}\right)_\zeta = \frac{u_\star}{3\varepsilon}, \tag{2.62}$$

$$\left(\frac{\partial u_\star}{\partial \zeta}\right)_\varepsilon = u_\star\left(\frac{d}{3(1+d(-\zeta)^{2/3})(-\zeta)^{1/3}}\right), \tag{2.63}$$

$$\left(\frac{\partial M}{\partial \varepsilon}\right) = -2M/\varepsilon. \tag{2.64}$$

2.E Individual terms in $S_{u_\star,z}$ for unstable conditions ($\zeta < 0$)

$$\left(\frac{\partial u_\star}{\partial z}\right)_\zeta = \frac{u_\star}{3z}, \tag{2.65}$$

$$\left(\frac{\partial u_\star}{\partial \zeta}\right)_z = u_\star\left(\frac{d}{3(1+d(-\zeta)^{2/3})(-\zeta)^{1/3}}\right), \tag{2.66}$$

$$\left(\frac{\partial M}{\partial z}\right) = 2M/z. \tag{2.67}$$

2.F Total differential expansion as in Andreas (1992) for unstable conditions ($\zeta < 0$)

Here we reproduce the analysis of *Andreas* [1992]. Subscripts indicate the equation that is being differentiated locally. The coupled equations are

$$\zeta = \frac{zgk}{u_\star^2 T}(T_\star + \frac{0.61T}{\rho + 0.61q}q_\star), \tag{2.68}$$

$$\varepsilon = \frac{u_\star^3}{\kappa z}\phi(\zeta) = \frac{u_\star^3}{\kappa z}(1 + d(-\zeta)^{2/3})^{3/2}, \tag{2.69}$$

$$T_\star = \frac{(1-b\zeta)^{1/3}z^{1/3}}{\sqrt{(a)}}\left(\frac{\text{sign}_1\sqrt{C_{n_1}^2}B_2 - \text{sign}_2\sqrt{C_{n_2}^2}B_1}{A_1B_2 - A_2B_1}\right), \tag{2.70}$$

$$q_\star = \frac{(1-b\zeta)^{1/3}z^{1/3}}{\sqrt{(a)}}\left(\frac{\text{sign}_2\sqrt{C_{n_2}^2}A_1 - \text{sign}_1\sqrt{C_{n_1}^2}A_2}{A_1B_2 - A_2B_1}\right). \tag{2.71}$$

We expand Eqs. 2.68 and 2.69 as

$$d\zeta = \left(\frac{\partial\zeta}{\partial z}\right)_{2.68}dz + \left(\frac{\partial\zeta}{\partial T_\star}\right)_{2.68}dT_\star + \left(\frac{\partial\zeta}{\partial q_\star}\right)_{2.68}dq_\star, \tag{2.72}$$

$$d\varepsilon = \left(\frac{\partial\varepsilon}{\partial u_\star}\right)_{2.69}du_\star + \left(\frac{\partial\varepsilon}{\partial z}\right)_{2.69}dz + \left(\frac{\partial\varepsilon}{\partial\zeta}\right)_{2.69}d\zeta. \tag{2.73}$$

Combining these, we obtain

$$
\begin{aligned}
d\varepsilon = &\left[\left(\frac{\partial \varepsilon}{\partial u_\star}\right)_{2.69} + \left(\frac{\partial \varepsilon}{\partial \zeta}\right)_{2.69}\left(\frac{\partial \zeta}{\partial u_\star}\right)_{2.68}\right] du_\star \\
&+ \left[\left(\frac{\partial \varepsilon}{\partial z}\right)_{2.69} + \left(\frac{\partial \varepsilon}{\partial \zeta}\right)_{2.69}\left(\frac{\partial \zeta}{\partial z}\right)_{2.68}\right] dz \\
&+ \left(\frac{\partial \varepsilon}{\partial \zeta}\right)_{2.69}\left(\frac{\partial \zeta}{\partial T_\star}\right)_{2.68} dT_\star \\
&+ \left(\frac{\partial \varepsilon}{\partial \zeta}\right)_{2.69}\left(\frac{\partial \zeta}{\partial q_\star}\right)_{2.68} dT_\star, \qquad (2.74)
\end{aligned}
$$

$$
\begin{aligned}
\frac{d\varepsilon}{\varepsilon} = &\frac{u_\star}{\varepsilon}\frac{du_\star}{u_\star}\left[\left(\frac{\partial \varepsilon}{\partial u_\star}\right)_{2.69} + \left(\frac{\partial \varepsilon}{\partial \zeta}\right)_{2.69}\left(\frac{\partial \zeta}{\partial u_\star}\right)_{2.68}\right] \\
&+ \frac{z}{\varepsilon}\frac{dz}{z}\left[\left(\frac{\partial \varepsilon}{\partial z}\right)_{2.69} + \left(\frac{\partial \varepsilon}{\partial \zeta}\right)_{2.69}\left(\frac{\partial \zeta}{\partial z}\right)_{2.68}\right] \\
&+ \frac{T_\star}{\varepsilon}\frac{dT_\star}{T_\star}\left(\frac{\partial \varepsilon}{\partial \zeta}\right)_{2.69}\left(\frac{\partial \zeta}{\partial T_\star}\right)_{2.68} \\
&+ \frac{q_\star}{\varepsilon}\frac{dq_\star}{q_\star}\left(\frac{\partial \varepsilon}{\partial \zeta}\right)_{2.69}\left(\frac{\partial \zeta}{\partial q_\star}\right)_{2.68}, \qquad (2.75)
\end{aligned}
$$

where the local derivatives are given by

$$\left(\frac{\partial \varepsilon}{\partial u_\star}\right)_{2.69} = \frac{3\varepsilon}{u_\star}, \tag{2.76}$$

$$\left(\frac{\partial \zeta}{\partial u_\star}\right)_{2.68} = \frac{-2\zeta}{u_\star}, \tag{2.77}$$

$$\left(\frac{\partial \varepsilon}{\partial \zeta}\right)_{2.69} = \frac{\varepsilon}{\phi(\zeta)}\frac{\partial \phi}{\partial \zeta}(\zeta), \tag{2.78}$$

$$\left(\frac{\partial \varepsilon}{\partial z}\right)_{2.69} = -\frac{\varepsilon}{z}, \tag{2.79}$$

$$\left(\frac{\partial \zeta}{\partial z}\right)_{2.68} = \frac{\zeta}{z}, \tag{2.80}$$

$$\zeta_T \equiv \frac{zg\kappa}{u_\star^2 T} T_\star, \tag{2.81}$$

$$\zeta_q \equiv \frac{zg\kappa}{u_\star^2 T}\left(\frac{0.61T}{\rho + 0.61q}\right) q_\star, \tag{2.82}$$

$$\zeta = \zeta_T + \zeta_q, \tag{2.83}$$

$$\left(\frac{\partial \zeta}{\partial T_\star}\right)_{2.68} = \frac{\zeta_T}{T_\star}, \tag{2.84}$$

$$\left(\frac{\partial \zeta}{\partial q_\star}\right)_{2.68} = \frac{\zeta_q}{q_\star}. \tag{2.85}$$

375 Thus the expansion becomes

$$\begin{aligned}\frac{d\varepsilon}{\varepsilon} = \frac{du_\star}{u_\star}&\left(3 - \frac{2\zeta}{\phi(\zeta)}\frac{\partial \phi}{\partial \zeta}(\zeta)\right) \\ &+ \frac{dz}{z}\left(-1 + \frac{\zeta}{\phi(\zeta)}\frac{\partial \phi}{\partial \zeta}(\zeta)\right) \\ &+ \frac{dT_\star}{T_\star}\frac{\zeta_T}{\phi(\zeta)}\frac{\partial \phi}{\partial \zeta}(\zeta) \\ &+ \frac{dq_\star}{q_\star}\frac{\zeta_q}{\phi(\zeta)}\frac{\partial \phi}{\partial \zeta}(\zeta),\end{aligned} \tag{2.86}$$

where $dT_\star$ and $dq_\star$ have been expanded in *Andreas* [1989] as

$$\frac{dT_\star}{T_\star} = S_z\frac{dz}{z} + S_{u_\star}\frac{du_\star}{u_\star} + S_{TC_{n_1}}\frac{dC_{n_1}}{C_{n_1}} + S_{TC_{n_2}}\frac{dC_{n_2}}{C_{n_2}}, \tag{2.87}$$

$$\frac{dq_\star}{q_\star} = S_z\frac{dz}{z} + S_{u_\star}\frac{du_\star}{u_\star} + S_{QC_{n_1}}\frac{dC_{n_1}}{C_{n_1}} + S_{QC_{n_2}}\frac{dC_{n_2}}{C_{n_2}}. \tag{2.88}$$

Thus we have

$$\frac{d_\varepsilon}{\varepsilon} = \frac{du_\star}{u_\star}\left(3 + \frac{\zeta}{\phi(\zeta)}\frac{\partial\phi}{\partial\zeta}(\zeta)(S_{u_\star} - 2)\right)$$
$$+\frac{dz}{z}\left(-1 + \frac{\zeta}{\phi(\zeta)}\frac{\partial\phi}{\partial\zeta}(\zeta)(S_z + 1)\right) + (\ldots)\frac{dC_{n_1}}{C_{n_1}} + (\ldots)\frac{dC_{n_2}}{C_{n_2}}, \tag{2.89}$$

which gives us

$$S_{u_\star,\varepsilon} = \frac{(1/3)}{(1 + \frac{1}{3}\frac{\zeta}{\phi(\zeta)}\frac{\partial\phi}{\partial\zeta}(\zeta)(S_{u_\star} - 2))}, \tag{2.90}$$

$$S_{u_\star,z} = \frac{\frac{1}{3}(1 - \frac{\zeta}{\phi(\zeta)}\frac{\partial\phi}{\partial\zeta}(\zeta)(S_z + 1))}{(1 + \frac{1}{3}\frac{\zeta}{\phi(\zeta)}\frac{\partial\phi}{\partial\zeta}(\zeta)(S_{u_\star} - 2))}, \tag{2.91}$$

where the terms $(S_{u_\star} - 2)$ and $(S_z + 1)$ are $(S_{u_\star} - 4)$ and $(S_z + 2)$ in *Andreas* [1992]. Eqs. 2.90
380 and 2.91 reduce to Eqs. 2.44 and 2.46. Also from *Andreas* [1989] we have

$$S_{u_\star} = \frac{2b\zeta}{3 - 2b\zeta}, \tag{2.92}$$

$$S_z = \frac{1 - 2b\zeta}{3 - 2b\zeta}, \tag{2.93}$$

where $S_{u_\star}$ would be denoted here as $S_{T_\star,u_\star}$ and S_z would be written here as $S_{T_\star,z}$ for a large-aperture scintillometer strategy not involving the derivation of $u_\star$ from Eq. 2.69. Eqs. 2.92 and 2.93 can be derived directly from the expressions in *Andreas* [1989] or they can be derived using the methodology outlined in this study. An alternative to using

the results from *Andreas* [1989] in Eqs. 2.87 and 2.88 is to perform the total-differential expansion in *Andreas* [1992] from all the equations including an expansion of Eqs. 2.70 and 2.71, although the results are the same as here.

Bibliography

Agarwal, R., M. Meehan, and D. O'Regan (2001), *Fixed Point Theory and Applications*, Cambridge University Press, Cambridge, United Kingdom, 184 pp.

Andreas, E. (1988), Estimating c_n^2 over snow and sea ice from meteorological data, *Journal of the Optical Society of America A*, *5*, 481–495.

Andreas, E. (1989), Two-wavelength method of measuring path-averaged turbulent surface heat fluxes, *Journal Of Atmospheric and Oceanic Technology*, *6*, 280–292.

Andreas, E. (1990), Three-wavelength method of measuring path-averaged turbulent heat fluxes, *Journal Of Atmospheric and Oceanic Technology*, *7(6)*, 801–814.

Andreas, E. (1992), Uncertainty in a path averaged measurement of the friction velocity $u_\star$, *Journal Of Applied Meteorology*, *31*, 1312–1321.

Andreas, E. (2012), Two experiments on using a scintillometer to infer the surface fluxes of momentum and sensible heat, *Journal Of Applied Meteorology and Climatology*, *doi: 10.1175/JAMC-D-H-0248-1*, in press.

Beyrich, F., H. de Bruin, W. Meijninger, J. Schipper, and H. Lohse (2002), Results from one-year continuous operation of a large aperture scintillometer over a heterogeneous land surface, *Boundary Layer Meteorology*, *105*, 85–97.

de Bruin, H., W. Meijninger, A.-S. Smedman, and M. Magnusson (2002), Displaced-beam small aperture scintillometer test. Part 1: The WINTEX data-set, *Boundary Layer Meteorology*, *105*, 129–148.

Edwards, H. (1984), *Galois Theory*, Springer Graduate Texts in Mathematics, 185 pp.

Foken, T., M. Mauder, C. Liebethal, F. Wimmer, F. Beyrich, J.-P. Leps, S. Raasch, H. de Bruin, W. Meijninger, and J. Bange (2008), Energy balance closure for the LITFASS 2003 experiment, *Theoretical Applied Climatology*, *101*, 149–160.

Hartogensis, O., H. de Bruin, and B. Van de Wiel (2002), Displaced-beam small aperture scintillometer test. Part II: CASES-99 stable boundary-layer experiment, *Boundary Layer Meteorology*, *105*, 149–176.

Hartogensis, O., C. Watts, J.-C. Rodriguez, and H. de Bruin (2003), Derivation of an effective height for scintillometers: La Poza experiment in Northwest Mexico, *Journal Of Hydrometeorology*, *4*, 915–928.

Hill, R. (1988), Comparison of scintillation methods for measuring the inner scale of turbulence, *Journal Of Applied Optics*, *27(11)*, 2187–2193.

Hill, R. (1989), Implications of monin-obukhov similarity theory for scalar quantities, *Journal of Atmospheric Science*, *46*, 2236–2244.

Hill, R., G. Ochs, and J. Wilson (1992), Heat and momentum using optical scintillation, *Boundary Layer Meteorology*, *58*, 391–408.

Hoedjes, J., R. Zuurbier, and C. Watts (2002), Large aperture scintillometer used over a homogeneous irrigated area, Partly affected by regional advection, *Boundary Layer Meteorology*, *105*, 99–117.

Kleissl, J., J. Gomez, S.-H. Hong, J. Hendrickx, T. Rahn, and W. Defoor (2008), Large aperture scintillometer intercomparison study, *Boundary Layer Meteorology*, *128*, 133–150.

Lagouarde, J., J. Bonnefond, Y. Kerr, K. McAneney, and M. Irvine (2002), Integrated sensible heat flux measurements of a two-surface composite landscape using scintillometry, *Boundary Layer Meteorology*, *105*, 5–35.

Liu, S., Z. Xu, W. Wang, Z. Jia, M. Zhu, J. Bai, and J. Wang (2011), A comparison of eddy-covariance and large aperture scintillometer measurements with respect to the energy balance closure problem, *Hydrological and Earth System Sciences*, *15*, 1291–1306.

Marx, A., H. Kunstmann, D. Schuttemeyer, and A. Moene (2008), Uncertainty analysis for satelite derived sensible heat fluxes and scintillometer measurements over savannah environment and comparison to mesoscale meteorological simulation results, *Agricultural Forest Meteorology*, *148*, 656–667.

Mason, P. (1988), The formation of areally-averaged roughness lengths, *Quarterly Journal of the Royal Meteorological Society*, *114*, 399–420.

Meijninger, W., O. Hartogensis, W. Kohsiek, J. Hoedjes, R. Zuurbier, and H. de Bruin (2002), Determination of area-averaged water vapour fluxes with a large aperture scintillometer over a heterogeneous surface - Flevoland field experiment, *Boundary Layer Meteorology*, *105*, 63–83.

Moroni, C., A. Navarra, and R. Guzzi (1990), Estimation of the turbulent fluxes in the surface layer using the inertial dissipative method: A Monte Carlo error analysis, *Boundary Layer Meteorology*, *50*, 339–354.

Panofsky, H., and J. Dutton (1984), *Atmospheric Turbulence: Models and Methods for Engineering Applications*, J. Wiley, New York, United States, 397 pp.

Press, W., S. Teukolsky, W. Vetterling, and B. Flannery (1992), *Numerical Recipes in Fortran: The Art of Scientific Computing, 2nd Edition*, Cambridge University Press, Cambridge, United Kingdom, 963 pp.

Sasiela, R. (1994), *Electromagnetic Wave Propagation in Turbulence: Evaluation and Application of Mellin Transforms*, Springer-Verlag, 300 pp.

Sokolnikoff, I. (1939), *Advanced Calculus*, McGraw-Hill Book Company, New York, United States, 446 pp.

Solignac, P., A. Brut, J.-L. Selves, J.-P. Béteille, J.-P. Gastellu-Etchegorry, P. Keravec, P. Béziat, and E. Ceschia (2009), Uncertainty analysis of computational methods for deriving sensible heat flux values from scintillometer measurements, *Journal Of Atmospheric Measurement Techniques*, *2*, 741–753.

Sorbjan, Z. (1989), *Structure of the Atmospheric Boundary Layer*, Prentice Hall, New Jersey, United States, 317 pp.

Tatarskii, V. (1961), *Wave Propagation in a Turbulent Medium*, McGraw-Hill Book Company, New York, United States, 285 pp.

Taylor, J. (1997), *An Introduction to Error Analysis: The Study of Uncertainties in Physical Measurements, 2nd Edition*, University Science Books, California, United States, 327 pp.

Traub, J. (1964), *Iterative Methods for the Solution of Equations*, Prentice-Hall, New Jersey, United States, 310 pp.

Wieringa, J. (1976), Roughness-dependent geographical interpolation of surface wind speed averages, *Quarterly Journal of the Royal Meteorological Society*, *112*, 867–889.

Wyngaard, J., and O. Coté (1971), The budgets of turbulent kinetic energy and temperature variance in the atmospheric surface layer, *Journal of Atmospheric Science*, *28*, 190–201.

Wyngaard, J., Y. Izumi, and S. Collins Jr (1971), Behavior of the refractive index structure parameter near the ground, *Journal of Optical Society of America*, *61*, 1646–1650.

3 Conclusions

3.1 Sensitivity of Turbulent Fluxes to Uncertainties in Source Measurements

Compact sensitivity functions have been produced which map the uncertainty propagation from source measurements to derived variables for various scintillometer strategies. This was accomplished by mapping out the variable inter-dependency such that partial derivatives could be evaluated directly using a combination of explicit and implicit differentiation with the use of the chain rule guided by tree diagrams. This is in contrast to total differential expansion techniques such as in *Andreas* [1989] or numerical Monte Carlo techniques such as in *Moroni et al.* [1990].

For homogeneous and flat terrain, the sensitivity functions produced in chapter 2 are functions of ζ only. Sensitivity functions for H_S, τ, and $u_\star$ as functions of ε and z were produced for a displaced beam scintillometer strategy. The sensitivity functions produced are lower in magnitude than the same sensitivity functions produced in *Andreas* [1992], especially in the range of $\zeta < -1$. The sensitivity functions produced here are compatible with the results of *Moroni et al.* [1990]. The sensitivity of H_S as a function of z for a large aperture scintillometer strategy was also investigated and found to be slightly overestimated in *Hartogensis et al.* [2003].

3.2 Validation of Flux Retrieval Techniques

Validating optical scintillometers for a role of retrieving large scale area averaged turbulent fluxes is difficult for two main reasons. Firstly, all scintillation measurement techniques involve the combination of measurements which are representative of various spacial scales. Tracking of uncertainty originating from the assumption of the representativity

of variables such as temperature on the beam path scale may be difficult. Sensitivity functions for variables such as temperature can be produced. While we have not produced these sensitivity functions here, we argue that as long as their values are not extremely low, taking this uncertainty into account may be important in interpreting plots such as Figures (4) and (5) in *Andreas* [2012]. In these plots, the functions $g(z/L)$ and $\phi(z/L)$ are evaluated with scintillometer data combined with eddy covariance data for $T_\star$, $u_\star$, and L. These independent measurements must be included since the evaluation of $T_\star$, $u_\star$ and L through scintillometer measurements alone forces $g(z/L)$ and $\phi(z/L)$ to be satisfied regardless of whether these functions represent reality. At least some of the scatter in 2012 Figures (4) and (5) must be due to the effect of varying scales of representativity of eddy-covariance measurements of $u_\star$ and $T_\star$ compared to scintillometer measurements of C_T^2. Future studies should investigate the difficulty of varying temperature along the beam path.

3.3 Analytic Solution of Equations and Computation of Turbulent Fluxes

Of the three types of error which are possible in experiments, random error is unavoidable, systematic instrumentational error can be calibrated out (or taken into account if it's due to measurements which are representative of varying scales), and computational error should be eliminated to the point of being at least several orders of magnitude smaller than systematic errors. Solution of the coupled set of Monin-Obukhov equations using the classical iterative algorithm may result in computational error. As illustrated in *Press et al.* [1992], it is generally impossible to bracket a solution in multiple dimensions, and pursuing a solution via iteration on nonlinear equations can result in circulating around solutions, stopping at a bottleneck, or diverging.

By reducing the set of equations into a single implicit equation in ζ, the solution can be found to arbitrary accuracy. The resulting implicit equation in ζ may be below fifth order, in which case explicit solutions can be derived [e.g., *Edwards*, 1984], or it may be above fifth order or non-algebraic. In any case, it was found to be practical to manipulate the

equations into fixed point form in a way which guarantees rapid monotonic convergence with fixed point recursion. The computer code involved with this solution method is very simple and compact.

3.4 Extension to Variable Topography and Heterogeneous Terrain

Complications of scintillometry include the fact that real field sites are likely to demonstrate variable topography and heterogeneous surface conditions such as roughness length, temperature, and water availability. This is difficult for the reason that the Monin-Obukhov hypothesis is based on stationary flow over flat terrain with homogeneous surface properties. Homogeneous conditions involve constant fluxes throughout the surface layer, while heterogeneous conditions involve gradients in the fluxes [e.g., *Sorbjan*, 1989; *Meijninger et al.*, 2002]. Fluxes over patches of terrain with differing roughness length, temperature, or water availability may be different from neighboring patches, although above a certain height the gradients in the fluxes dissipate. If the beam is above this "blending height" then it can be safely assumed that height profiles of C_T^2, for instance, satisfy the Monin-Obukhov hypothesis [e.g., *Meijninger et al.*, 2002]. The blending height is the height at which the internal boundary layers of each individual terrain patch blend to become indistinguishable from adjacent patches, thus dissolving any horizontal gradients in fluxes [e.g., *Wieringa*, 1976; *Mason*, 1988; *Claussen*, 1990; *Braden*, 1995; *Claussen*, 1995; *Meijninger et al.*, 2002; *Hartogensis et al.*, 2003; *Stoll*, 2007; *Lu et al.*, 2009]. Even if the height profiles of structure functions can be assumed to satisfy the Monin-Obukhov hypothesis at any point over the terrain via the assumption of stationary turbulence over terrain with homogeneous surface properties (or a beam above the blending height over heterogeneous terrain) and negligible effects due to air interaction with terrain gradients, the beam is still sampling turbulence at variable heights above the underlying terrain.

The next simplest theoretical field site from a flat and homogeneous one is one with variable topography, homogeneous surface properties such as roughness length and temperature, weak topographic gradients and stationary flow. Equivalent to this is a site with variable topography and heterogeneous surface properties, but with a beam which is in-

stalled above the blending height under stationary flow conditions. It is still assumed that the turbulent fluxes are constant within the surface layer (or above the blending height), but it is assumed that C_T^2 obeys the height dependency reflected in Eq. (1.7) at all points above the underlying topography (or above the blending height). The beam thus samples regions with different intensities of C_T^2 along its path. In addition, scintillometers are optically more sensitive to fluctuations in the index of refraction near the center of the line between the transmitter and receiver [e.g., *Ochs and Wang*, 1974; *Hartogensis et al.*, 2003]. To take this into account, *Hartogensis et al.* [2003] rewrote Eq. (1.7) as

$$\overline{C_T^2} = T_\star^2 g(z_{eff}/L) {z_{eff}}^{-2/3} \tag{3.1}$$

where $\overline{C_T^2}$ is a single value of C_T^2 which is measured by the scintillometer, and z_{eff} is the effective beam height which is a single value of height representative of the entire measurement area. In order to resolve the effective beam height in order to use $\overline{C_T^2}$ in Monin-Obukhov equations based on flat terrain, the C_T^2 field along the beam path is considered as

$$C_T^2(u) = T_\star^2 g(z(u)/L) z(u)^{-2/3} \tag{3.2}$$

where u is the normalized distance along the beam between the transmitter and receiver and $C_T^2(u)$ is the actual C_T^2 field along the beam path [e.g., *Hartogensis et al.*, 2003]. The assumption behind Eq. (3.2) is effectively that the height profile of C_T^2 assumed through the Monin-Obukhov similarity hypothesis obeys Eq. (1.7) at any point above the actual variable topography, and that L is representative of the constant flux surface layer. The effective height z_{eff} is a function of the terrain profile represented by $z(u)$, the optical path weighting function, and L in a way which can be determined by equating $\overline{C_T^2}$ in Eq. (3.1) to the single value of C_T^2 which is measured by the scintillometer in Eqs. (1.9) and (1.10) [e.g., *Hartogensis et al.*, 2003; *Kleissl et al.*, 2008]. If the effect of humidity fluctuations on the index of refraction fluctuations is negligible, then Eq. (1.10) relates C_n^2 to C_T^2 linearly; it can then be derived that

$$\overline{C_T^2} = \int_0^1 C_T^2(u) G(u) du \tag{3.3}$$

where G is an area-normalized optical path weighting function derived from Eq. (1.9) (or from a corresponding equation for a different type of scintillometer) [e.g., *Ochs and Wang*, 1974; *Hartogensis et al.*, 2003]. Eqs. (3.1) and (3.2) can be substituted into Eq. (3.3) to solve for the effective beam height z_{eff} in equations such as (3.1) by

$$g\left(\frac{z_{eff}}{L}\right) {z_{eff}}^{-2/3} = \int_0^1 g\left(\frac{z(u)}{L}\right) z(u)^{-2/3} G(u) du \tag{3.4}$$

as seen in *Hartogensis et al.* [2003] and *Kleissl et al.* [2008]. This allows the use of the value of $C_T^2 = \overline{C_T^2}$ in similarity equations for flat terrain as long as $z = z_{eff}$ is input for the single value of air sample height. Note that it has been assumed that other variables such as a temporally averaged temperature are constant along the beam path, i.e., $T(u) = T$. It has also been assumed that there is a constant flux layer [e.g., *Hartogensis et al.*, 2003], thus the beam should ideally be above the blending height if the surface demonstrates heterogeneous properties, although for moderately heterogeneous surfaces *Meijninger et al.* [2002] have determined that a beam below the blending height still measures reliable fluxes.

The approach described above was derived in *Hartogensis et al.* [2003] and *Kleissl et al.* [2008]; it involves line integral equations to take into account variable terrain under stationary turbulence, with a beam above the blending height. It is important to note that, if the terrain is variable enough to have a high blending height, more complicated theory may be required. In order to further take into account the variable topography and heterogeneous surface conditions in general over a two dimensional field with arbitrary wind strength and direction as well as significant topographical gradients, it is natural to consider surface integrals instead of line integrals. This type of analysis is often described as resolving the "footprint" of the scintillometer; it is described in, for example, *Meijninger et al.* [2002].

Future work should establish whether computational error can be eliminated in the case of variable terrain, and the sensitivity of turbulent fluxes to $z(u)$ should be established for both large aperture and displaced-beam scintillometer strategies. One would imagine that, since the flat terrain sensitivity functions for z are functions of ζ only, then the variable terrain sensitivity functions for $z(u)$ will be functions of both u and ζ.

Bibliography

Andreas, E. (1989), Two-wavelength method of measuring path-averaged turbulent surface heat fluxes, *Journal Of Atmospheric and Oceanic Technology*, *6*, 280–292.

Andreas, E. (1992), Uncertainty in a path averaged measurement of the friction velocity $u_\star$, *Journal Of Applied Meteorology*, *31*, 1312–1321.

Andreas, E. (2012), Two experiments on using a scintillometer to infer the surface fluxes of momentum and sensible heat, *Journal Of Applied Meteorology and Climatology*, *doi: 10.1175/JAMC-D-H-0248-1*, in press.

Braden, H. (1995), Energy fluxes from heterogeneous terrain: averaging input paraters of the Penman-Monteith formula, *Agricultural and Forest Meteorology*, *75*, 121–133.

Claussen, M. (1990), Area-averaging of surface fluxes in a neutrally stratified, horizontally inhomogeneous atmospheric boundary layer, *Atmospheric Environment*, *24A*, 1349–1360.

Claussen, M. (1995), Flux aggregation at large scales: on the limits of validity of the concept of blending height, *Journal of Hydrology*, *166*, 371–382.

Edwards, H. (1984), *Galois Theory*, Springer Graduate Texts in Mathematics, 185 pp.

Hartogensis, O., C. Watts, J.-C. Rodriguez, and H. de Bruin (2003), Derivation of an effective height for scintillometers: La Poza experiment in Northwest Mexico, *Journal Of Hydrometeorology*, *4*, 915–928.

Kleissl, J., J. Gomez, S.-H. Hong, J. Hendrickx, T. Rahn, and W. Defoor (2008), Large aperture scintillometer intercomparison study, *Boundary Layer Meteorology*, *128*, 133–150.

Lu, L., S. Liu, Z. Xu, K. Yang, X. Cai, L. Jia, and J. Wang (2009), The characteristics and parameterization of aerodynamic roughness length over heterogeneous surfaces, *Advances in Atmospheric Science*, *26*, 180–190.

Mason, P. (1988), The formation of areally-averaged roughness lengths, *Quarterly Journal of the Royal Meteorological Society*, *114*, 399–420.

Meijninger, W., O. Hartogensis, W. Kohsiek, J. Hoedjes, R. Zuurbier, and H. de Bruin (2002), Determination of area-averaged water vapour fluxes with a large aperture scintillometer over a heterogeneous surface - Flevoland field experiment, *Boundary Layer Meteorology*, *105*, 63–83.

Moroni, C., A. Navarra, and R. Guzzi (1990), Estimation of the turbulent fluxes in the surface layer using the inertial dissipative method: A Monte Carlo error analysis, *Boundary Layer Meteorology*, *50*, 339–354.

Ochs, G., and T.-I. Wang (1974), Finite aperture scintillometer for profiling wind and C_n^2, *Journal of Applied Optics*, *17*, 3774–3778.

Press, W., S. Teukolsky, W. Vetterling, and B. Flannery (1992), *Numerical Recipes in Fortran: The Art of Scientific Computing, 2nd Edition*, Cambridge University Press, Cambridge, United Kingdom, 963 pp.

Sorbjan, Z. (1989), *Structure of the Atmospheric Boundary Layer*, Prentice Hall, New Jersey, United States, 317 pp.

Stoll, J. (2007), Surface heteorogeneity effects on turbulent fluxes in the atmospheric boundary layer, Ph.D. thesis, University of Minnesota.

Wieringa, J. (1976), Roughness-dependent geographical interpolation of surface wind speed averages, *Quarterly Journal of the Royal Meteorological Society*, *112*, 867–889.

4 Glossary of Terms

a, b, c, d, e	empirical constants
β	Bowen ratio
c_p	specific heat capacity
C_n^2	index of refraction structure function
C_T^2	temperature structure function
C_Q^2	humidity structure function
D	thermal diffusivity
ε	turbulent energy dissipation rate
f	derived variable
g	acceleration of gravity
Γ	Γ function
H_S	sensible heat flux
H_L	latent heat flux
k	optical wavenumber
K	turbulence spacial wavenumber
κ	Von Kármán constant
L	Obukhov length
λ	electromagnetic wavelength
l_o	inertial subscale length
L_p	beam propagation distance
L_v	latent heat of vaporization
ν	viscosity

p	pressure
ϕ	similarity function
Ψ_m	similarity function
Ψ_n	turbulence spectrum function
ρ	density
q	humidity
$q_\star$	humidity scale
R	specific gas constant
T	temperature
$T_\star$	temperature scale
τ	momentum flux
$u_\star$	friction velocity
u	East-West wind velocity
v	North-South wind velocity
w	up-down wind velocity
x	source measurement
z	height above ground
z_o	roughness length
z_{eff}	effective beam height